RIGA TECHNICAL UNIVERSITY

Ģirts Staņa

MODELLING OF ELECTRIC TRANSPORT OVERHEAD DC LINES FOR MOBILE ENERGY STORAGE SYSTEM OPTIMIZATION

Summary of the Doctoral Thesis

RTU Press
Riga 2024

RIGA TECHNICAL UNIVERSITY
Faculty of Computer Science, Information Technology and Energy
Institute of Industrial Electronics and Electrical Engineering

Ģirts Staņa
Doctoral Student of the Study Program "Computerised Control of Electrical Technologies"

MODELLING OF ELECTRIC TRANSPORT OVERHEAD DC LINES FOR MOBILE ENERGY STORAGE SYSTEM OPTIMIZATION

Summary of the Doctoral Thesis

Scientific supervisor
Associate Professor Dr. sc. ing.
VIESTURS BRAŽIS
Consultant
Senior Researcher Dr. sc. ing.
KASPARS KROIČS

RTU Press
Riga 2024

Staņa, G. Modelling of Electric Transport Overhead DC Lines for Mobile Energy Storage System Optimization. Summary of the Doctoral Thesis. – Riga: RTU Press, 2024. – 50 p.

Published in accordance with the decision of Promotion Council "P-14" of 14 February 2024, Minutes No. 33400-4/1.

This research has been supported by Riga Technical University's Doctoral Grant Programme; Project 4421, "Studying colour reconnection effects on top quark mass measurements using colour flow observables – preparing the study for Run 3 of the CMS experiment of the CERN LHC," lzp-2020/2-0228; and Project 4588, "Fast transient response and high-efficiency GaN-based BLDC motor converter with a dual power supply," lzp-2021/1-0298.

FLPP
FUNDAMENTĀLO UN LIETIŠĶO PĒTĪJUMU PROJEKTI

1862
RĪGAS TEHNISKĀ UNIVERSITĀTE

Cover picture from www.shutterstock.com

https://doi.org/10.7250/9789934370694
ISBN 978-9934-37-069-4 (pdf)

DOCTORAL THESIS PROPOSED TO RIGA TECHNICAL UNIVERSITY FOR PROMOTION TO THE SCIENTIFIC DEGREE OF DOCTOR SCIENCE

To be granted the scientific degree of Doctor of Science, the present Doctoral Thesis has been submitted for defence at the open meeting of RTU Promotion Council on June 19, 2024 at the Faculty of Computer Science, Information Technology and Energy of Riga Technical University, Azenes street 12/1, room 212.

OFFICIAL REVIEWERS

Professor Dr. sc. ing. Iļja Galkins
Riga Technical University

Associate Professor Dr. habil. sc. ing. Mikolaj Bartlomiejczyk,
Gdansk University of Technologies, Poland

Associate Professor Dr. sc. ing. Pavel Drabek
University of West Bohemia, Czech Republic

DECLARATION OF ACADEMIC INTEGRITY

I hereby declare that the Doctoral Thesis submitted for review to Riga Technical University for promotion to the scientific degree of Doctor of Engineering Sciences is my own. I confirm that this Doctoral Thesis has not been submitted to any other university for promotion to a scientific degree.

Ģirts Staņa ……. (signature)
Date: ……

The Doctoral Thesis has been written in Latvian. It consists of an Introduction, 4 chapters, Conclusions, 151 figures, and 9 tables; the total number of pages is 145. The Bibliography contains 58 titles.

CONTENTS

INTRODUCTION

Public electric transport infrastructure, as an integral part of any developed country's capital and other major cities, is one of the largest electricity consumers. Therefore, improving of energy efficiency of public electric transport infrastructure by reducing electricity consumption is a topical issue. Research on improving the energy efficiency of public electric transport, such as trolleybuses, might not always be possible using real vehicles as they might be unavailable, for example. Therefore, the use of virtual computer models can be an alternative [1], [2]. The application of energy storage systems (ESS) in public electric transport has so far been the subject of both studies based on practical experiments using real vehicles [3], [4], [5] and studies with computer simulation models of electric transport vehicles and ESS [6], [7]. The modelling of operations of electric transport vehicles and their ESS can be performed in multiple virtual environments such as PSIM [8], [9] and Matlab Simulink [10], [11]. However, the theoretical studies conducted until now on the application of ESS for electric transport have several drawbacks which are addressed in this work. For example, no studies have been conducted on the additional amount of energy that a rolling stock is forced to consume due to additional supercapacitor (SC) ESS mass and whether this energy consumption increase is significant considering the amount of recoverable braking energy.

The variable overhead transmission resistance, which depends on the distance between the supply substation and the vehicle, has often been assumed to be constant over the entire motion cycle [12], [13]. In frames of certain studies, also models in which the overhead resistance varies section by section with respect to a moving vehicle have been developed [14]. Therefore, to ensure that the simulation results are as accurate as possible to the real-world situations, the models in which the overhead catenary line transmission resistance, that is between the supply substation and the moving trolleybus, changes dynamically in real time according to the trolleybus location along the overhead catenary line were developed in this research. While studies have usually considered internal losses in substations by using resistor elements that imitate certain resistance or losses in the substation transformer and rectifier, internal losses in traction drive inverters and ESS DC/DC converters have often not been considered.

Studies [15] and [16] have presented methods for estimating the unused recoverable regenerated energy of electric vehicles using real experimental data on the consumed and regenerated power of electric trams using probabilistic and statistical methods. The efficiency of the recovery of regenerated energy depends on the permissible power intensity and energy capacity of the SC ESS. This allows to calculate the savings by considering the payback period of a specific ESS and the total energy savings over the ESS service life. However, the authors acknowledged that for more accurate recoverable energy estimations, transmission losses along the overhead catenary and losses in ESS should also be considered [17].

In the absence of the possibility to use real public electric vehicles for research where a vehicle is equipped with SC ESS, stationary traction drive test benches are also often used, usually consisting of two electric machines coupled together, one simulating the traction of the vehicle and the other simulating the load [18], [19]. However, the power scales of such benches are usually considerably lower than those of real vehicles, so the results of experiments

performed on these benches cannot be considered as completely accurate even if proportionality is ensured.

No previous studies have been performed on the reduction of SC ESS efficiency during its lifetime caused by the worsening of electrical parameters. SC equipment works most efficiently when it is brand new but according to manufacturers' information on SC ageing, the SC electrical performance degrades more and more with each next charge/discharge cycle. During the lifetime of the equipment, this ageing can have a significant impact on the efficiency of regenerated braking energy storage, as at some point, the energy capacity of the ESS might have decreased to such a level that the ESS can no longer store all the energy regenerated by the electric vehicle. This research, therefore, outlines the need to consider the impact of ageing to obtain more objective estimation results for the long-term profitability and payback of ESS.

Mobile ESS can also be charged from overhead catenary and the basic charging methods are constant-current and constant-power charging. Theoretical studies have been performed on the charging/discharging of SC circuits with constant power based on the RC (resistor-capacitor) model that is most widely used for SC modelling [20]. However, no previous studies have evaluated which SC charging/discharging method is more efficient – constant current or constant power. Therefore, this research compares SC charging/discharging with constant current and SC charging/discharging with constant power under equal boundary conditions, i.e. in both cases charging and discharging occur from the same initial voltages to the same final voltages during equal times. These comparisons were made based on the RC circuit.

Goals and objectives of the Thesis

1. Develop transmission loss improved modelling methods for motion simulations of public electric transport – trolleybus – that is connected to overhead catenary.
2. Develop a method to determine the amount by which the available energy capacity of economical mobile SC ESS should be higher than the maximum regenerated energy considering that the energy capacity of SC cells decreases during operational lifetime.
3. Perform simulations to explore how the mobile SC ESS mass affects the energy consumption of the trolleybus traction drive and whether this increase is more than 5 % and is significant compared to the recovered braking energy.
4. Develop a method to approximate the amount of supply substation energy saved during the lifetime of the SC ESS, the financial value of which can be compared with the purchase cost of the SC ESS to analyse the full payback and return of the ESS.
5. Compare SC ESS discharge control strategies aimed at ensuring that ESS, in combination with the substation, can supply the traction drive until the end of acceleration, thus avoiding the substation power peak due to ESS getting discharged.

Hypotheses

1. The increase in trolleybus drive energy consumption due to the additional mass of a mobile SC ESS is below 5 %.
2. In an RC (resistor-capacitor series connection) circuit that is intended as an equivalent replacement of an SC circuit, charging with constant current is as efficient as charging

with constant supplied power if there are equal charging conditions, i.e. the charging occurs over equal time durations and over equal voltage ranges in both methods. Similarly, discharging with constant current is as efficient as discharging with constant power at the SC output if there are equal discharging conditions in both methods.

Scientific novelties

1. A method for calculating consumer voltage and current in real time at known consumer power, transmission resistance and source voltage by deriving quadratic equations and logically finding the correct roots of the solutions was developed. A similar method for calculating the transmission voltage drop compensation current, the purpose of which is to ensure that the required power is provided to the consumer, was developed.
2. Three algorithms for real-time simulation of overhead catenary transmission resistance between the supply substation and the moving trolleybus were developed: with mathematical calculation of electrical parameters; with application of virtual resistor elements; and with application of virtual voltage source elements.
3. A method to simulate in real time the mobile SC ESS DC/DC converter operation results without modelling the converter's internal processes and commutations was developed.
4. A method to determine the amount by which the initial energy capacity of a mobile SC ESS should be higher than the maximum regenerated energy so that the regenerated energy is efficiently stored and used over the entire lifetime of the ESS, considering the SC ageing and losses in both DC/DC converter and inverter, was developed.
5. Simulation results showed that the additional mass of mobile ESS results in an increase in trolleybus drive energy consumption of less than 5%, which is insignificant compared to the regenerated energy that is successfully stored and used thanks to the ESS.
6. Mobile SC ESS discharge strategies aimed to ensure that the ESS can supply the trolleybus drive until the end of the acceleration mode to avoid the substation power peak were developed and compared.
7. A method to calculate the approximate amount of saved substation energy and its total cost over the entire ESS lifetime was developed, finding that more significant ESS payback and return occurs at higher electricity prices rather than at lower ESS purchase costs.
8. Analytical expressions were derived by comparing RC circuit-based SC constant-current charge/discharge and constant-power charge/discharge under equal charge/discharge conditions, and calculations showed that constant-current case is more efficient than constant-power case, but the difference is usually less than 1 %.

Approbation of the work

The Doctoral Thesis results were presented in totally 32 (thirty-two) published works, including three scientific journal articles, one collective monograph, and 28 conference publications which were presented in 26 scientific conferences in Latvia (9), Estonia (5), Russia (4), Romania (3), Czech Republic (2), Turkey (1), Bulgaria (1), and Lithuania (1).

1. MODELLING OF THE OPERATIONAL PROCESSES OF MOBILE SUPERCAPACITOR ENERGY STORAGE SYSTEMS FOR PUBLIC ELECTRIC TRANSPORT

Modern electric public transport units (including trolleybuses) are equipped with regenerative electric drives that operate as electric power generators during braking, thereby generating additional electric energy known also as braking or regenerated energy. Trolleybuses have brake resistors where regenerated energy is dissipated in heat if it cannot be stored. Since trolleybuses brake rather frequently during their operation, especially in intensive urban traffic conditions, quite significant amounts of regenerated energy are generated. It is, therefore, worth considering options to make efficient use of this regenerated energy, and the main one is the application of ESS.

In Riga and many other cities, non-reversible rectifiers in traction substations only provide a one-way flow of power, so the regenerated power cannot be fed from the substation back to the high-voltage AC grid. The regenerated energy can be transmitted to another trolleybus that moves along the same section of overhead catenary, but it is not frequently that when one trolleybus brakes, another trolleybus, which is in the same catenary section, accelerates. In addition, the accelerating trolleybus might not absorb all the regenerated power of the decelerating trolleybus because the amount of power demanded at a certain moment might be less than the regenerated power. Therefore, it can be assumed that in the absence of ESS, most of the regenerated energy is dissipated in brake resistors.

Two types of ESS can be used to store and use recovered energy: mobile ESS, which is installed in the transport itself (called mobile because the transport moves together with it) and stationary ESS, which is installed in a supply substation or connected to a catenary outside the substation (called stationary because it does not move but remains in one place only).

Mobile ESS do not cause power transmission losses, but their main disadvantage is the additional load on the trolleybus due to the higher mass of the trolleybus caused by the mobile ESS. As a result, the trolleybus traction drive consumes more energy when moving compared to a situation without this additional load. On the other hand, it was studied and confirmed that this disadvantage is compensated by the fact that the amount of energy, that is previously stored in ESS during braking and used during the next acceleration, significantly reduces the substation's total energy consumption compared to the situation when all the regenerated energy is dissipated in brake resistors. However, in the case of an existing but non-functioning mobile ESS, the total energy consumption of the substation during trolleybus operation is clearly higher due to the higher drive energy consumption and, consequently, higher transmission losses.

In the case of stationary ESS, the trolleybus is not subject to additional load, but power transmission losses are present. The transmission losses of the energy taken from stationary ESS and the transmission losses of the energy transmitted to stationary ESS are variable depending on the distance between the trolleybus and the stationary ESS.

The main advantages of using ESS are:

- lower power consumption from the substation and lower overhead catenary load;

- lower transmission losses;
- lower substation total energy consumption.

In a 2004 paper [21], which is one of the first to consider the use of ESS in electric transport, a proposal was presented to connect stationary SC-based ESS, even referred to as SC substation, to the overhead catenary of electric transport with the aim of reducing the voltage drop of the catenary with respect to the moving transport vehicle. The locations where these stationary SC substations are to be connected to the overhead catenary, e.g. at the endpoints of the overhead catenary section, have been defined as the weak or sensitive points located furthest from the substation because there are correspondingly higher transmission losses and the voltage there can drop from 700 V to as low as 350 V at high power demands when several electric transport vehicles start accelerating at the same time (meanwhile, the voltage of the substations in Riga is 600 V, so the voltage of any section of the overhead catenary is 600 V when there are no loads). Besides, modern AC traction drive systems are not designed for significant input voltage fluctuations, so the use of stationary ESSs is seen as a pragmatic solution. It is mentioned that regenerative braking is a typical feature of new and improved transport vehicles of that time, such as trolleybuses, trams, and metros. However, most substations are non-reversible, which means that the regenerated energy is not transmitted back to the high-voltage AC grid. This leads to the use of resistors where the regenerated energy is dissipated in heat, but no mention is made of the possibility of transmitting the regenerated energy to another accelerating transport vehicle in the same overhead catenary section. The first ESSs were installed on the London underground using rotating kinetic energy technologies [22], [23]. The first SC-based ESSs were installed in Cologne, Germany [24].

In [25], simulation-based studies on the efficiency of ESS have been performed, concluding that mobile ESS reduces the substation's total energy consumption by 24–27.6 % on average, while at the end of the ESS SC service life, this consumption is by 18.1–25.1 % lower, depending on the SC modules used. It has been recommended to choose ESS with an energy capacity that is equal to the amount of regenerated energy. It is mentioned and shown how, in the very last phase of ESS service life, its electrical parameters have worsened, and its energy capacity has decreased, so that part of the regenerated energy is dissipated in brake resistors. Also, in [12], the efficiency of the ESS at the very end of its service life, i.e. at the millions charge/discharge cycle, has been shown, but the efficiency over the entire lifetime of the ESS, e.g. after the first 30 000, 50 000, 200 000 cycles, etc., have not been analysed. However, it has not been recommended that ESS should be selected with an energy capacity that is at a certain percentage higher than the regenerated energy, aiming that over the entire lifetime of the SC equipment, their energy capacity is sufficient to avoid the need to dissipate part of the regenerated energy in brake resistors. Therefore, the Thesis describes a planning and calculation method for the SC ESS aiming to determine the required ESS capacity and the number of SC cells so that the ESS energy capacity does not decrease during the SC lifetime to the level at which there is insufficient space to store all the regenerated energy.

Reference [7] analyses the impact of the ESS DC/DC converter efficiency on the amount of saved energy but it does not analyse the impact of the traction drive inverter efficiency on the amount of saved energy. As with the DC/DC converter, the regenerated energy flows

through the traction inverter twice during one full ESS charge/discharge cycle. It is, therefore, understandable that for more accurate energy saving studies, it would be recommended to also consider the impact of inverter efficiency on the amount of saved energy. Therefore, the impact of both the ESS DC/DC converter efficiency and the traction drive inverter efficiency on the effectiveness of the regenerated energy recovery is studied in this work.

1.1. Losses during the recovery of regenerated energy

Figure 1.1 shows a diagram of the trolleybus regenerated energy recovery process or "life cycle" to explain how all possible losses of regenerated energy were considered according to their sequence of occurrence. During ESS charging, the regenerated energy flows through the traction inverter and the DC/DC converter, while during ESS discharging, the successfully stored energy flows back to the traction drive through the same devices. Therefore, it can be concluded that the efficiency of the traction inverter and the DC/DC converter can have a significant impact on the overall efficiency of the regenerated energy recovery, especially because during a full ESS charge/discharge cycle the energy flows through each device twice.

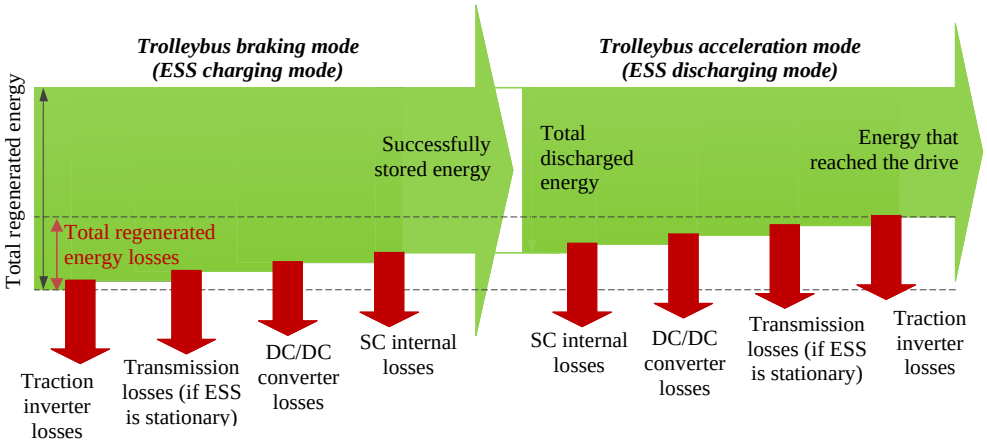

Fig.1.1. Trolleybus regenerated energy recovery life cycle diagram.

In addition to the traction drive, trolleybus has a variety of other energy-consuming equipment such as lighting, door opening/closing, etc., but in general, this equipment consumes insignificant amounts of energy compared to the energy consumed by the traction drive. However, air-conditioning systems in summer and heating systems in winter can consume significant amounts of energy. During braking, part of the regenerated energy is automatically used to supply the mentioned self-consumption equipment. Further work assumed that neither the air conditioning nor the heating systems are operating in the trolleybus when it is moving.

1.2. Method of modelling the operation results of DC/DC converter for supercapacitor energy storage system

DC/DC converters differ in capabilities and complexity of design but their basic principles of operation are generally similar. In the simplified schematics shown in Fig. 1.2, the converter is divided into two parts or sides, of which one is connected to the DC grid (left) and the other is connected to the SC circuit (right). Hereafter, the SC circuit must be understood as a multiple SC cell circuit which is equivalently replaced by capacitor and resistor series circuit (RC circuit). The capacitance C corresponds to the total capacitance of all SC cells while the resistance R_c corresponds to the total active resistance of all SC cells. These parameters are calculated according to corresponding formulas depending on how SC cells are connected.

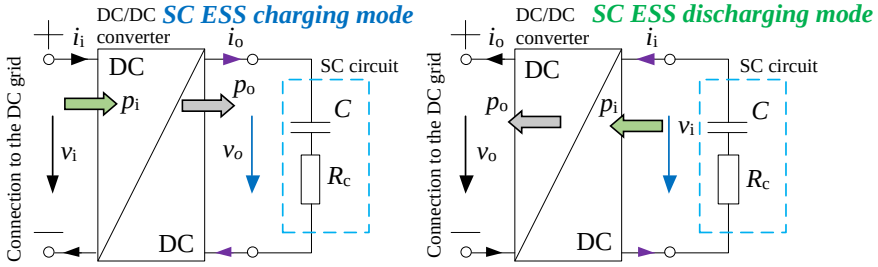

Fig.1.2. Current and power flow at the input and output of the DC/DC converter.

It is usually considered that the converter's input is the side into which power flows and the output is the side from which power flows. Thus, in ESS charging mode, the converter's side connected to the grid is the input and the side connected to the SC circuit is the output. In ESS discharging mode, the converter's side connected to the SC circuit is the input and the side connected to the grid is the output.

The basic principle of an ideal DC/DC converter is that its input power, $p_{i,}$ is equal to its output power, p_o. It means that in such a lossless situation the product of the input side current i_i and voltage v_i is equal to the product of the output side current i_o and voltage v_o:

$$i_i v_i = i_o v_o \,. \tag{1.1}$$

However, in a real situation, the converter has internal losses the amount of which can be estimated from its efficiency η. Due to internal losses, the output power p_o is always lower than the input power p_i since $\eta < 1$. This can be described by the following relation:

$$p_o = \eta p_i. \tag{1.2}$$

Therefore, Expression (1.1) must be modified by including the converter efficiency η, thus obtaining the actual relationship between the converter input and output currents and voltages:

$$i_o v_o = \eta i_i v_i. \tag{1.3}$$

Figure 1.3 shows a model diagram of a trolleybus connected to an overhead catenary and equipped with mobile ESS. U1 is a voltage source for simulating the overhead voltage drop.

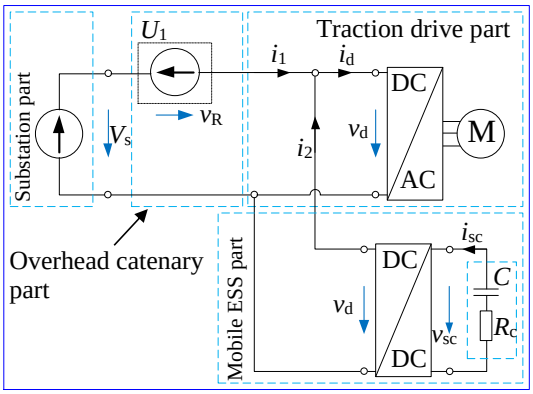

Fig. 1.3. Simplified block diagram of a model of trolleybus equipped with mobile ESS.

To avoid simulating the commutation processes of the DC/DC converter, a virtual model of the trolleybus motion was developed where the ESS charging and discharging are simulated by current source elements using two unconnected block diagrams, as in Fig. 1.4 showing the ESS discharge case. The diagram on the left simulates the overhead catenary side in relation to the DC/DC converter, while the diagram on the right simulates the SC side in relation to the DC/DC converter. It means that the converter itself is not simulated but the results of its operation are obtained.

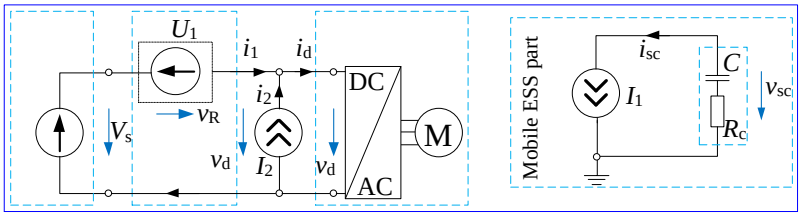

Fig. 1.4. Simplified circuit of two unconnected block diagram models of overhead catenary-connected trolleybus equipped with mobile SC ESS.

It is worth mentioning that in Fig.1.4, the drive part with inverter and motor M can be replaced by a current source, making the model simpler. In this case, the power profile of the trolleybus drive must be known in advance and prepared in the form of a time-dependent power graph. Using the known drive power, the corresponding drive current is calculated in real time and applied to the trolleybus simulating the current source as the division of drive power and drive voltage.

During the charging process, both current sources in Fig. 1.4 have opposite directions of current flow compared to the shown ones and the power p_i that is successfully delivered to the DC/DC converter is lower than the total regenerated power p_d due to inverter losses. Hence, p_i is calculated by the formula:

$$p_i = \eta_{inv} p_d, \tag{1.4}$$

where η_{inv} is the efficiency of the traction inverter.

Therefore, the current to be applied to the current source I_2 is calculated according to (1.5):

$$i_2 = \frac{p_\mathrm{i}}{v_\mathrm{d}}\,. \tag{1.5}$$

The power passed through the DC/DC converter, i.e. the power p_{sc} on the converter's SC side is lower than the input power p_i due to converter losses. So, p_{sc} is calculated by (1.6):

$$p_\mathrm{sc} = \eta_\mathrm{con} p_\mathrm{i}\,, \tag{1.6}$$

where η_{con} is the efficiency of the DC/DC converter.

The converter's SC side current to be applied to the current source I_1 is calculated by (1.7):

$$i_\mathrm{sc} = \frac{p_\mathrm{sc}}{v_\mathrm{sc}}\,, \tag{1.7}$$

where v_{sc} is the SC circuit voltage that is measured during simulation.

The model must also include an algorithm controlling the SC ESS state of charge during the simulation. As soon as the SC ESS is charged to the maximum permissible voltage level, the charging must be stopped by not applying current to sources I_1 and I_2. If the SC ESS charging is stopped, the power that is still regenerating is dissipated in heat. The algorithm considers the capacitor element's C voltage which is the actual SC circuit state-of-charge voltage. Due to the internal resistance R_{SC}, the SC circuit voltage measured with a voltmeter is slightly higher than the actual voltage when charging but lower when discharging.

In the case of SC ESS discharge, a condition might be imposed specifying what part of the total drive power is taken from the substation and what part is taken from the SC ESS. Then, the current to be applied to the current source I_2 is calculated according to the formula:

$$i_2 = \frac{k p_\mathrm{d}}{v_\mathrm{d}} = \frac{p_2}{\mathrm{v_d}}, \tag{1.8}$$

where k is the coefficient that determines what portion of the drive power p_d is the power p_2 taken from the SC ESS.

The power on the converter's SC side is calculated considering the losses in both the DC/DC converter and in the traction inverter using the formula:

$$p_\mathrm{sc} = \frac{p_2}{\eta_\mathrm{inv}\eta_\mathrm{imp}}. \tag{1.9}$$

The formula of applied current for the source I_1 is calculated by (1.7) also in the discharging case. In addition, the model must also contain an algorithm controlling the SC ESS state of discharge. As soon as the SC ESS is discharged to the minimum permissible voltage level, the discharging must be stopped by not applying current to sources I_1 and I_2. If the SC ESS discharging is stopped, all the power required for the traction drive is taken from the substation.

2. NEW APPROACHES FOR CALCULATING AND SIMULATING TRANSMISSION LOSSES IN ELECTRIC TRANSPORT OVERHEAD DC CATENARY GRID

Calculation and simulation-based research on the energy efficiency of an electric transport connected to an overhead catenary, such as a trolleybus, must consider losses in overhead catenary during power transmission. As the trolleybus moves, its position in the overhead catenary section changes continuously, and therefore the overhead catenary resistance between the substation and the trolleybus is a variable parameter.

2.1. Calculation of overhead catenary electrical resistance between the substation and moving vehicle

The trolleybus must be connected to a pair of two contact wires, i.e. positive (+) polarity and negative (–) polarity to ensure power flow from the substation to the trolleybus drive. Most streets used by trolleybuses have two-way or bi-directional traffic, so each lane has its own pair of (+) and (–) polarity overhead contact wires. In most cases, the possibility of connecting those two contact wire pairs in parallel with current stabilising wires is always used, thus reducing the transmission resistance. The described situation is shown in Fig. 2.1, where the (+) and (–) polarity wires of both lanes are connected in parallel. The resistors R_S symbolise the resistances of the overhead wire sections. The trolleybus drive is represented in the schematic by an inverter and an AC motor. It was further assumed that the overhead catenary stage consists of 200 m long sections and that each section wire resistance R_S = 0.0354 Ω, assuming that the wires are MF-100 with 100 mm^2 cross-sectional area and specific resistance $\rho = 1.77 \cdot 10^{-8}$ Ωm.

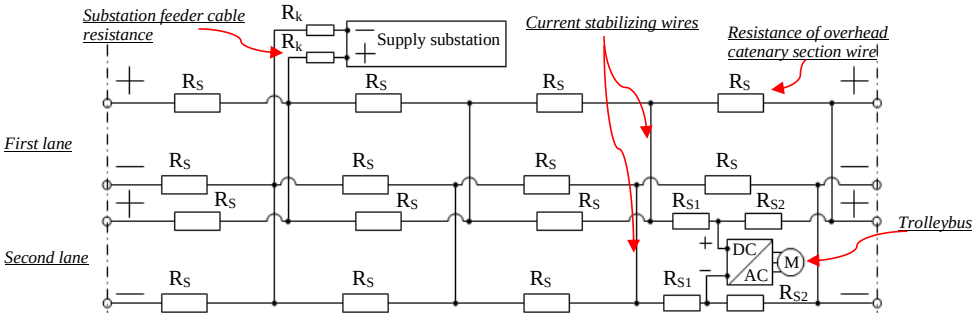

Fig. 2.1. Electrical circuit diagram of a two-way overhead catenary stage.

The resistor circuit in Fig. 2.1 can be simplified to one resistor R, which represents the total transmission resistance R of the overhead catenary between the substation and the trolleybus as shown in Fig. 2.3, where the trolleybus drive is replaced by a current source D and the substation is replaced by voltage source S. The corresponding expression for the resistance R is

$$R = 2R_{\mathrm{k}} + aR_{\mathrm{s}} + R_{\mathrm{s}}\left(\frac{x}{d}\right)\left(2 - \frac{x}{d}\right) = 2R_{\mathrm{k}} + R_{\mathrm{s}}\left(a + \left(\frac{x}{d}\right)\left(2 - \frac{x}{d}\right)\right), \qquad (2.1)$$

where

a – the coefficient denoting the number of sections before the trolleybus location section;

x – the trolleybus position coordinate in the section (from 0 m to 200 m), m;

d = 200 m – the length of the overhead catenary section in which the trolleybus is located;

R_k – resistance of the substation feeder cable, Ω.

Figure 2.2 shows how the resistance according to (2.1) increases section by section. In this case, R_k is not considered, assuming that the trolleybus is very close to the substation.

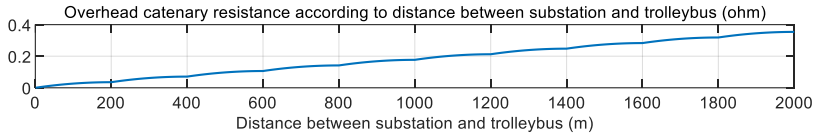

Fig. 2.2. Overhead catenary resistance between the substation and the trolleybus.

2.2. Calculation of consumer voltage and current at known transmission line parameters and consumer power

The situation with one energy consumer can be described by the circuit shown in Fig. 2.3, where the current source D is the consumer, the resistor R is the transmission resistance, and S is the voltage source. It is further assumed that the consumer D is a trolleybus consuming power P = 200 kW, the source S is a substation of voltage V_S = 600 V, and transmission resistance R = 0.2 Ω. Known parameters are depicted in green while the unknown ones are in red.

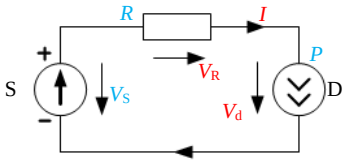

Fig. 2.3. Electrical circuit with the voltage source, consumer, and transmission resistance.

Mathematical calculation with derivation of quadratic equations

The situation in Fig. 2.3 can be formulated as a problem with the following conditions:

Given: P = 200 kW; V_S = 600 V; R = 0.2 Ω.

Calculate: I = ?; V_d = ?; V_R = ?

Although the circuit in Fig. 2.3 is elementary, solving the given problem is not that simple as it consists of several steps and requires reasoning. First, the system of three equations with Ohm's and Kirchhoff's laws on which the circuit operation is based must be written:

$$\begin{cases} P = IV_d \\ V_R = IR \\ V_S = V_R + V_d \end{cases}. \tag{2.2}$$

Since the Equation system (2.2) consists of three equations and three unknowns, it is mathematically solvable. But in the process of solving, the quadratic equations are derived. From (2.2), the quadratic Equation (2.3) for calculating the current I, the quadratic equation for

calculating the voltage drop V_R and the quadratic Equation (2.5) for calculating the consumer voltage V_d can be derived:

$$RI^2 - V_S I + P = 0, \tag{2.3}$$

$$V_R^2 - V_S V_R + RP = 0, \tag{2.4}$$

$$V_d^2 - V_S V_d + RP = 0. \tag{2.5}$$

Because of quadratic equations, there are two calculation formulas for each of the parameters I, V_R and V_d. This raises the question of which is the correct one for each parameter, since, for example, the current I cannot have two different numerical values at the same time. If an equation system has several solutions, then from a mathematical point of view, there are several options under which the system is valid. As an example, Fig. 2.4 shows two electrical circuit variants at which the Equation system (2.2) is valid. Under each circuit, the corresponding solution roots of quadratic equations are written, while the calculated numerical values are indicated for the corresponding parameters in the electrical circuits.

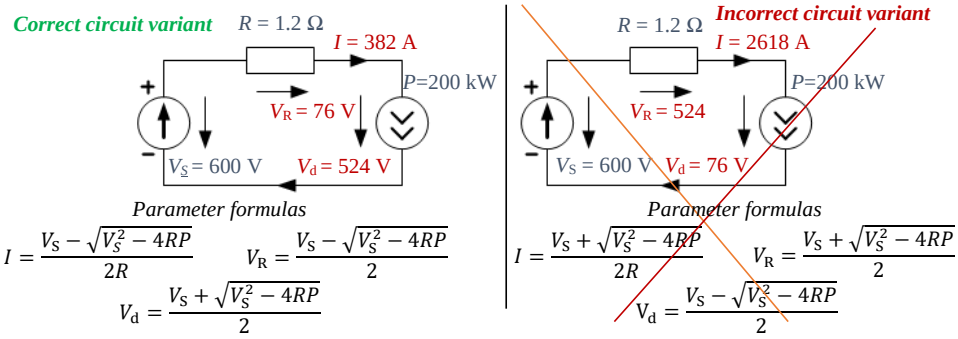

Fig. 2.4. Two electrical circuit variants for which the Equation system (2.2) is valid.

In Fig. 2.4, it is visible that in the "wrong" variant, V_R and V_d have their positions swapped in comparison to the "right" variant, and that is the reason why the current I is very high. Although the problem solution is based on elementary mathematics, the resulting multiple solutions might cause certain confusion meaning that the correct roots of solutions must be determined by logical reasoning. For example, the value of V_R cannot be higher than V_d, so the correct root of (2.4) has a (–) sign and (2.5) has a (+) sign before the square root. The current of 2618 A is too high for the trolleybus drive current, so the correct root of (2.3) has a (–) sign before the square root. It is advisable to add at least one of the mentioned statements as a comment in the description of this type of problem when assigned to students in frames of field-related subjects. The quadratic equations and their solution roots cannot be called general physics or electrical circuit calculation formulas, but without their derivation, the problem cannot be solved in written form. In fact, it is quite enough to derive the quadratic equation of just one parameter – I, V_R or V_d – and solve the value of its correct root because the remaining parameters can be calculated using the generally known formulas, as shown in Table 2.1.

Table 2.1

Calculation of Electrical Circuit Parameters

	Parameter that is calculated using the root of quadratic equation		Remaining parameters that are calculated using general formulas
Variant I	$I = \frac{V_S - \sqrt{V_S^2 - 4RP}}{2R}$	⇨	$V_R = IR\,; \quad V_d = V_s - V_R$
Variant II	$V_R = \frac{V_S - \sqrt{V_S^2 - 4RP}}{2}$	⇨	$I = \frac{V_R}{R}; \quad V_d = V_s - V_R$
Variant III	$V_d = \frac{V_S + \sqrt{V_S^2 - 4RP}}{2}$	⇨	$V_R = V_s - V_d\,; \quad I = \frac{V_R}{R}$

Variant with calculation of transmission loss compensation current

This method in comparison to the previous one is rather similar but provides additional insight how the transmission losses are compensated by stronger current. It can be assumed that in the Equation system (2.2), the current I includes two components: the ideal current I_{id}, which corresponds to the case with no transmission losses, and the additional current $I_{C,}$ which compensates the voltage drop V_R, thus providing the required drive power P. Regardless of the trolleybus location, the power P for certain speed will remain the same. If the overhead catenary was without resistance, the drive voltage V_d would be equal to the substation voltage V_S. Therefore, the following two-equation system can be written for calculating I_C and V_R:

$$\begin{cases} P = I_{id}V_s = IV_d = (I_{id} + I_c)(V_s - V_R) \\ V_R = (I_{id} + I_c)R \end{cases}. \tag{2.6}$$

From (2.6), the quadratic Equation (2.7) for calculating I_C can be derived and the correct root (2.8) obtained, as well as the quadratic Equation (2.9) for calculating V_R and the correct root (2.10) obtained:

$$I_c^2 R + I_c(2I_{id}R - V_s) + I_{id}^2 R = 0, \tag{2.7}$$

$$I_c = \frac{-2I_{id}R + V_s - \sqrt{V_s(V_s - 4I_{id}R)}}{2R}, \tag{2.8}$$

$$V_R^2 - V_s V_R + I_{id}V_s R = 0, \tag{2.9}$$

$$V_R = \frac{V_s - \sqrt{V_s(V_s - 4I_{id}R)}}{2}. \tag{2.10}$$

Expressions (2.9), (2.10), and expressions from Fig. 2.4 can be solved if the values of their sub-roots or discriminants are greater than or equal to zero. The case with discriminant equal to zero is at the maximum resistance R in the situation where the voltages V_R and V_d are each half of the substation voltage V_S. In the trolleybus case, the V_d can drop to the minimum voltage of V_{d_min} = 400 V, which is higher than half of V_S = 600 V.

2.3. Options for modelling overhead transmission losses

Three methods of modelling transmission losses during trolleybus motion simulation are described. In all models, the transmission resistance R is calculated by (2.1) during simulation.

Transmission loss modelling using mathematical calculation of electrical parameters

The model in Fig. 2.5 includes a circuit without transmission resistance simulating resistor and operating in an ideal lossless mode with flowing current I_{id} and drive voltage V_d that is equal to substation voltage V_S. During model operation, the actual current I, voltage drop V_R, drive voltage V_d, transmission loss power P_R, substation power P_S, transmission loss energy E_R, and substation energy E_S are calculated using a separate block. There are two options to calculate the unknowns of I, V_R and V_d: real time measurement of drive power P and using (2.2) solutions; real time measurement of ideal mode current I_{id} using (2.6) solutions. In Fig. 2.5, both option blocks with the corresponding input parameters are shown. It is possible to choose which option to use but their results are identical. The first option might be simpler in terms of complexity, but the second option allows to see how much the drive current must be increased to compensate for transmission losses. The right side of Fig. 2.5 shows the simulation results of the current of 27Tr filled with passengers in mode without losses (I_{id}) and in mode with losses (I), assuming that the 27Tr is initially 0.6 km from the substation and accelerated up to 50 km/h.

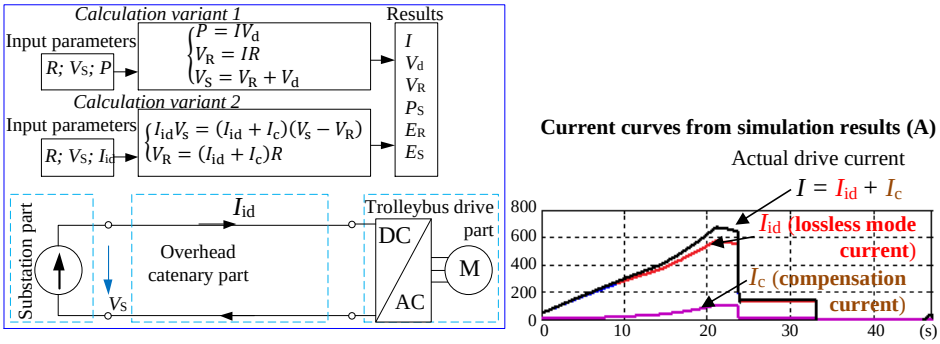

Fig. 2.5. Trolleybus motion model with parameter calculation and simulation results of current.

Transmission loss modelling using a resistor element circuit

The left side of Fig. 2.6 shows the schematic of the trolleybus catenary transmission loss simulation subsystem with a resistor circuit, and the right side shows the algorithm of this subsystem's operation with the conditions at which the corresponding switches must be closed. The resistor circuit shows the path of current flow (in red), based on an example with a trolleybus being 80 m – 120 m away from the substation, while the algorithmic diagram shows the cycle for this example (in red). The resistor circuit is controlled by the switches according to the trolleybus position coordinate X by switching the correct circuit of resistors corresponding to the transmission resistance R. Block A contains the resistor simulating substation feeder wire resistance, B contains resistors corresponding to transmission resistances R_S, and C contains resistors corresponding to transmission resistances of separate parts of the

catenary section. If the section length is 200 m, then the diagram in Fig. 2.6 is a variant where the transmission resistance is modified after every 40 m travelled by the trolleybus because part C contains 5 resistors. If it is decided to modify the resistance after every 1 m, then the number of resistors in part C must be 200, but then the model becomes more complex with a longer compilation time.

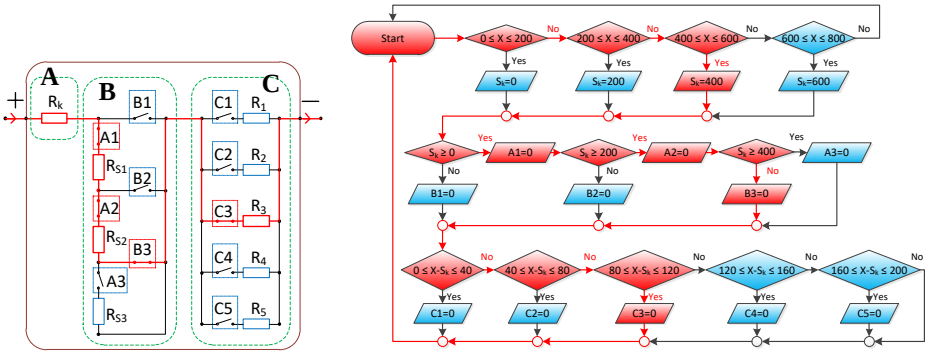

Fig. 2.6. Schematic of the resistor subsystem (left) and the algorithmic diagram for its control.

Figure 2.7 shows a simplified diagram of trolleybus motion model containing the subsystem R with a resistor circuit from Fig. 2.6 simulating the transmission resistance.

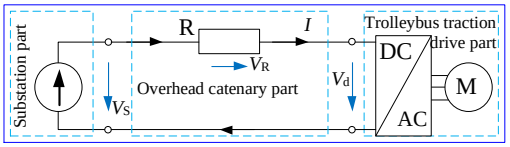

Fig. 2.7. Simplified block diagram of the trolleybus motion model with a resistor subsystem.

Transmission loss modelling using voltage source element

Resistors, which are passive elements, can be equivalently replaced by voltage sources, which are active elements. In this method, instead of the resistor subsystem, voltage source R is applied, as shown in Fig. 2.8. The source is assigned the value corresponding to the voltage drop V_R. During simulation, the ammeter measures the current I that is multiplied by the resistance R, thus obtaining the value corresponding to V_R. As in the model with the resistor subsystem, the voltage drop V_R is compensated automatically by a stronger current from the substation-simulating voltage source. This model operates according to real situations because, unlike the previous model where the resistance is modified in certain steps, in this case, the resistance is modified all the time depending on the distance travelled by the trolleybus.

For this model, the V_R calculation can also consider the compensation of trolleybus drive inverter losses, which are compensated by taking stronger current from the substation just like in the transmission loss compensation case, thus providing the required power at the inverter output. If the inverter efficiency is k, the formula for calculating V_R for the voltage source is

$$V_R = kI_d R. \tag{2.11}$$

This model has the important advantage of being considerably simpler than the ones described previously and does not contain complex calculation algorithms. Therefore, the two-trolleybus motion simulation described further was based on this model.

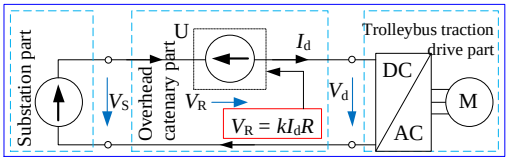

Fig. 2.8. A simplified diagram of the trolleybus motion model with voltage source element.

2.4. Calculation and modelling of electrical resistance of overhead catenary in the case of two-trolleybus motion

In trolleybus braking mode, its regenerated energy can be transmitted to another trolleybus, which is located in the same catenary stage and accelerates. In the absence of ESS, the braking trolleybus regenerated energy is automatically transmitted to the overhead catenary towards the direction of the accelerating trolleybus. When studying this option of using regenerated power, overhead catenary transmission resistance must be considered due to a certain distance between the two trolleybuses. Consequently, part of the regenerated power is lost due to transmission resistance and these losses will be higher at longer distances between the trolleybuses.

In the case of two trolleybuses, the substation can be connected to the overhead catenary between the two trolleybuses, as shown in Fig. 2.9 on the left, or to one of the end-points of the catenary stage, as shown on the right. In the first situation, the distribution of currents for each trolleybus when both are accelerating is the same as previously for a single trolleybus, excluding only the R_k part. However, in the second situation, the common current of both trolleybuses, T_1 and T_2, flows in the section between the substation and its nearest trolleybus, T_1. Due to the T_2 current, the catenary voltage drop in relation to T_1 is higher than in the absence of T_2, because, in T_1 point of view, the current for T_2 in the part between the substation and T_1 is a disturbing current, which causes an additional voltage drop. The same can be stated also for the T_1 current in relation to T_2.

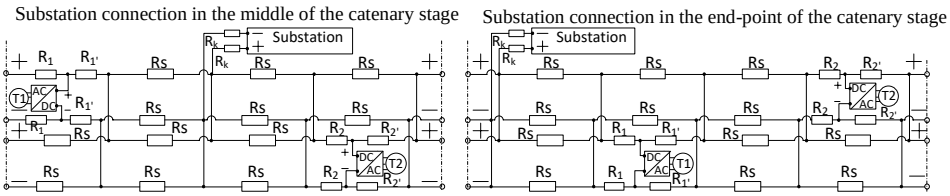

Fig. 2.9. Two-way overhead catenary schemes with two trolleybuses.

Further, the right-side circuit from Fig. 2.9 was considered and equivalently simplified, resulting in a three-resistor star connection circuit shown in Fig. 2.10. The corresponding formulas for the resistances of R_A, R_B and R_C are:

$$R_A = 2R_k + aR_s + R_s\left(\frac{x}{d}\right), \tag{2.12}$$

$$R_B = \frac{2R_1R_{1'}}{R_1 + R_{1'} + R_s} = R_s\left(\frac{x}{d}\right)\left(1 - \frac{x}{d}\right), \tag{2.13}$$

$$R_C = R_s\left(\left(1 - \frac{x}{d}\right) + b - (a+1) + \left(\frac{x'}{d}\right)\left(2 - \frac{x'}{d}\right)\right), \tag{2.14}$$

where

$x \in [0; 200]$ – the trolleybus T_1 location coordinate in the section, m;

$d = 200\ m$ – the length of the section in which trolleybus T_1 is located, m;

a – the coefficient denoting the number of sections before the trolleybus T_1 location section;

$x' \in [0; 200]$ – the trolleybus T_2 location coordinate in the section, m;

b – the coefficient denoting the number of sections before the trolleybus T_2 location section.

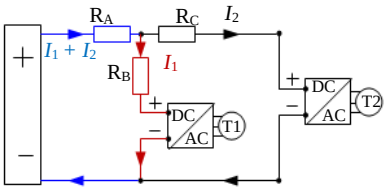

Fig. 2.10. A simplified electrical circuit of a two-way overhead catenary stage with two trolleybuses and a substation connected at the end-point of the catenary stage.

Transmission loss modelling using voltage source elements

Figure 2.11 shows the application of three voltage sources simulating the corresponding voltage drops in parts with resistances R_A, R_B, and R_C with an example where T_1 and T_2 both are accelerating. R_A, R_B, and R_C are calculated in real time according to the locations of two trolleybuses, while the currents of these parts are measured with virtual ammeters whose measurements are used to calculate the voltages to be applied to the sources. The formulas for calculating these voltage values are shown in the red frames. Eventually, the corresponding currents I_1 and I_2 from the substation voltage source are taken automatically at the existing trolleybus drive powers and voltage drops.

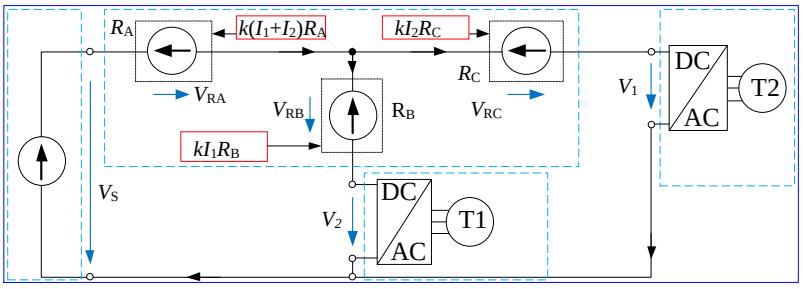

Fig. 2.11. Diagram of a two-trolleybus model with voltage source elements to simulate the voltage drop across overhead catenary when both trolleybuses are accelerating.

Interpretation of the trolleybus regenerative power flow simulation results

At the beginning of the simulation, T_1 is 0.2 km and T_2 is 1.4 km from the substation. T_1 starts accelerating to 50 km/h moving away from the substation. At the 30th second, also T_2 starts accelerating by moving away from the substation. After the 40th second, T_1 starts braking. Figure 2.12 shows the simulation results with several power diagrams. For visual clarity, the regenerated power of the braking T_1 is plotted in the positive value part of the number plane. Since the energy is calculated by integrating the power, the coloured areas in Fig. 2.12 represent certain energy quantities. When at the 30th second T_2 starts moving, the substation power consumption correspondingly increases. After the 40th second, it is visible that when T_1 starts braking, it regenerates more power than required by T_2, so part of this power is dissipated in brake resistors but substation power consumption immediately equals zero. As soon as T_1 regenerated less power than T_2 requires, the remaining power is taken from the substation. There might be countless examples of regenerated power transmission to accelerating trolleybus. The efficiency of this process is determined by the distance between the trolleybuses and the difference between the power regenerated and the power required by another trolleybus.

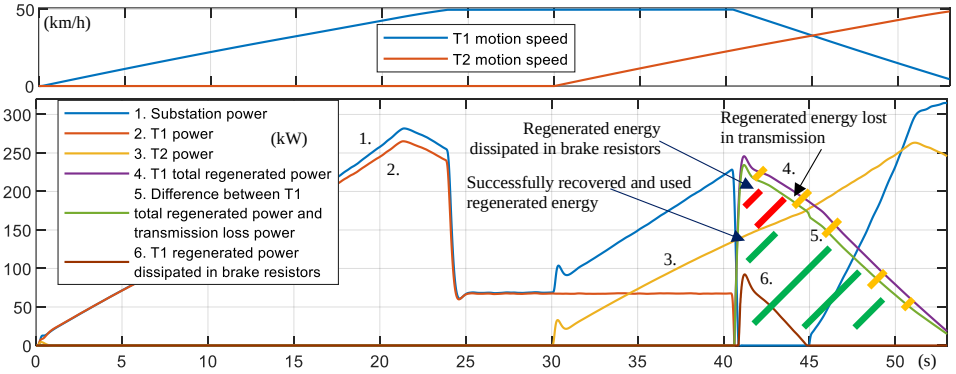

Fig. 2.12. The simulation result speed and power diagrams of the two-trolleybus motion.

2.5. Impact of overhead catenary temperature variation on transmission losses and substation energy consumption

Although in scientific and technical literature the temperature of materials is mostly assumed to be 20 °C for calculations of wire resistances, it is desirable not to forget that the specific resistance ρ of any material varies with temperature. In this case, the catenary resistance R that is calculated by (2.1) varies proportionally with variation of ρ. Therefore, at certain temperatures, the actual R is calculable using the reference resistance R_{ref} corresponding to the reference temperature T_{ref} = 20 °C, while the formula for calculating R at any temperature T is

$$R = R_{\text{ref}}[1 + \alpha(T - T_{\text{ref}})], \tag{2.15}$$

where α = 0.00393 is the copper resistance thermal coefficient.

It was further assumed that the same value applies to the MF-100 wire, meaning that the R increases by 0.393 % when the material temperature increases by 1°C. The motion of fully

loaded Škoda 27Tr with steady acceleration from 0 km/h to 50 km/h in 23.8 seconds was studied, comparing the amount of transmission loss energy E_Z and the substation total energy consumption E_S at 0 m, 500 m, and 1000 m initial distances between the substation and 27Tr. For each of the three distances, E_Z and E_S were compared at five different overhead catenary resistances calculated by (2.15) at the following temperatures: 10 °C, 20 °C, 30 °C, 40 °C, and 50 °C. If the 27Tr motion is considered for three different distances with five temperature variations each, then there are, in total, fifteen separate cases. To avoid fifteen simulations, numerical calculations were made using MS Excel.

Since in each of the 15 cases, the trolleybus speed curves are equal, the drive power curves are also going to be equal. However, before making further calculations, one simulation must be performed to obtain the drive power curve. If the time step for 23.8-second acceleration simulation is 0.005 s long, then, in total, 4760 drive power P_d values are generated (this number is obtained dividing 23.8 by 0.005), resulting in the power curve shown in Fig. 2.13.

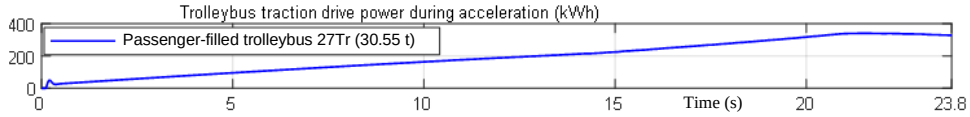

Fig. 2.13. A passenger-filled 27Tr drive acceleration power curve obtained by simulation.

The P_d numerical values are copied into an Excel document as an array consisting of one column with 4760 rows to perform further calculations which require five more columns with transmission resistance R values for different temperatures. Figure 2.14 shows R curves for five different temperatures when the initial distance between the trolleybus and the substation is 1 km. These curves can be obtained either from simulations or from calculations with (2.15) since the curve of the distance travelled by the trolleybus is calculable by using the speed curve.

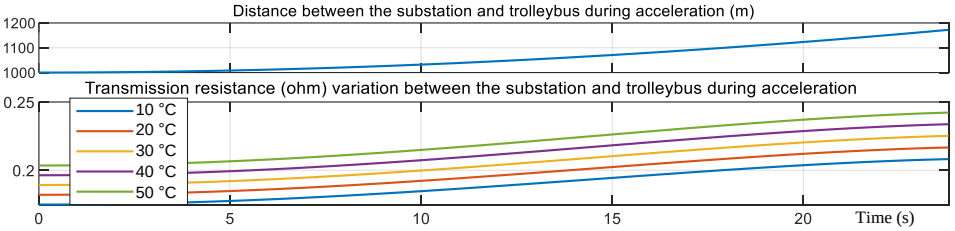

Fig. 2.14. Overhead catenary transmission resistances according to the distance between the trolleybus and the substation at five different wire temperatures.

The drive energy consumption E_d can be calculated for periods t = 0.005 s by (2.16):

$$E_d = P_d t. \tag{2.16}$$

In (2.16), the drive power P_d is capitalised because it is assumed to be constant at intervals of t = 0.005 s. The same applies to the drive current I and the drive voltage V_d. E_d is the energy that is consumed only in t = 0.005 s period with a certain constant P_d. The total drive energy that is consumed during acceleration E_D is the sum of separate E_d values calculated by (2.16):

$$E_{\mathrm{D}} = \sum_{\mathrm{n}=1}^{4760} P_{\mathrm{dn}} t = \sum_{\mathrm{n}=1}^{4760} E_{\mathrm{dn}}. \tag{2.17}$$

This situation is an example of the practical use of the current I calculation method by equations derived in subchapter 2.2 since further work requires calculating I for each of 4760 P_{d} values. The transmission loss energy E_{z} for any of 4760 P_{d} values can be calculated by

$$E_{\mathrm{z}} = I^2 R t. \tag{2.18}$$

In (2.18), t = 0.005 s, meaning that any E_{z} represents only the energy that is lost during a particular 0.005 s period with certain I and R. The total transmission loss energy E_{Z} during the entire 23.8 s of transmission is calculated as the sum of 4760 E_{z} values:

$$E_{\mathrm{Z}} = \sum_{n=1}^{4760} I_n^2 R_n t = \sum_{n=1}^{4760} E_{zn}. \tag{2.19}$$

It is also possible to obtain the substation power curve by calculating its power 4760 times for certain P_{d}, I, and R with t = 0.005 s using Formula (2.20):

$$P_{\mathrm{s}} = \frac{(I^2 R + P_{\mathrm{d}})t}{\eta_1 \eta_2}, \tag{2.20}$$

where η_1 is the efficiency of substation's transformer and η_2 is the efficiency of substation's rectifier.

The total substation energy E_{S} that is consumed in 23.8 s can be calculated with three different expressions written below with t = 0.005 s:

$$E_{\mathrm{S}} = \sum_{n=1}^{4760} \frac{(I_n^2 R_n + P_{\mathrm{dn}})t}{\eta_1 \eta_2} = \sum_{n=1}^{4760} \frac{(E_{zn} + E_{\mathrm{dn}})}{\eta_1 \eta_2} = \sum_{n=1}^{4760} P_{sn} = \frac{E_{\mathrm{Z}} + E_{\mathrm{D}}}{\eta_1 \eta_2}. \tag{2.21}$$

Figure 2.15 shows the E_{Z} and E_{S} values at different overhead temperatures concluding that an increase in overhead catenary temperature significantly increases the amount of E_{Z}, while the amount of E_{S} increases insignificantly, i.e. not reaching 5 %. It follows that the transmission loss energy forms a relatively small part of the substation's total energy consumption. Therefore, in the following studies on SC ESS design, the overhead catenary resistance was calculated assuming that wire temperature is 20 °C.

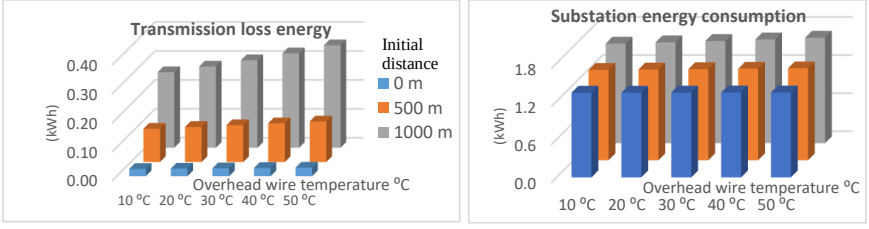

Fig. 2.15. Transmission loss energies and substation energies.

2.6. Experimental measurements of DC line parameter variations at consumer long-term constant power

So far, it has been described how the voltage drop and the flowing current change with the varying overhead length between the energy source and the consumer – trolleybus, resulting in the required traction power. Therefore, it was decided to test with the available equipment the increase of voltage drop V_R in the DC power transmission line caused by the increase of wire temperature when the consumer – electric motor – is operated at constant power for an extended time. Several experiments were performed at different DC line wire lengths and constant motor powers. These situations are comparable to stationary consumers, such as motors or industrial robots in factories and stopped electric transport, whose power sources are not in their close vicinity but at considerable distances. If the motor is switched on and the power starts flowing, the DC line conductors start to warm up gradually until their temperature reaches a certain value, T_{max}, at which it does not increase anymore, remaining constant unless the ambient temperature does not change either. The principal circuit of the bench is shown in Fig. 2.16 where the resistor R represents the total resistance of transmission line (+) and (–) wires.

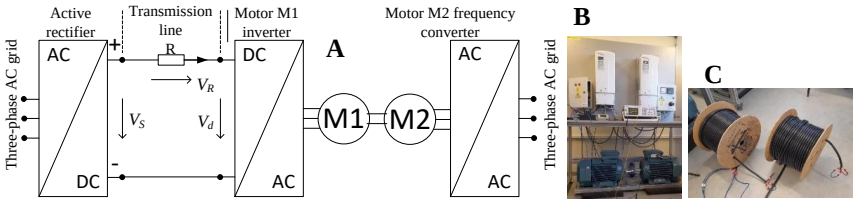

Fig. 2.16. A – circuit diagram for taking measurements; B – motor test bench; C – coiled cables.

The bench with two coupled motors, which was used, can also be considered a traction drive emulator, with M1 being the traction motor and M2 – the load motor. The measurements were taken in relation to M1 using two approximately 100 m long cables with four copper conductors of 6 mm^2 cross-sectional area, from which transmission lines of certain lengths were connected. At high currents, the cables must be uncoiled to ensure proper cooling. Otherwise, they can heat up to critically high temperatures with their insulations melting if coiled. The cables were uncoiled and deployed outside the laboratory room along the hallway floor, as in Fig. 2.17, also showing some images from the measurements taken with a thermographic camera. Long DC line temperature measurement in real-time is not an easy task as the temperature distribution might be uneven due to different conditions, i.e. some wire parts might have higher temperature and others lower. Therefore, the wire temperature was not measured in real time while the motor was running but the transmission line voltage drop was indirectly measured.

Fig. 2.17. Infrared and visible light images taken during experiments.

A power analyser was used to measure the line current I and the voltage V_d at the motor inverter input, while the power P_d at the motor inverter input was calculated as the product of the measured I and V_d. Measurements were taken every second, so a total of 2100 values of I, V_d and P_d were obtained in 35 minutes, producing characteristic curves for these parameters. Active rectifier voltage V_S = 600 V while the voltage drop V_R can be calculated as the difference between V_S and V_d. When V_d stops decreasing and V_R stops increasing, the maximum wire temperature, the approximate values of which were measured with a thermographic camera, can be considered as reached. The transmission resistance curves over 35-minute periods were obtained by dividing V_R by I. Figure 2.18 shows the measurement results of a 400 m long DC line at 15 kW and 20 kW motor power.

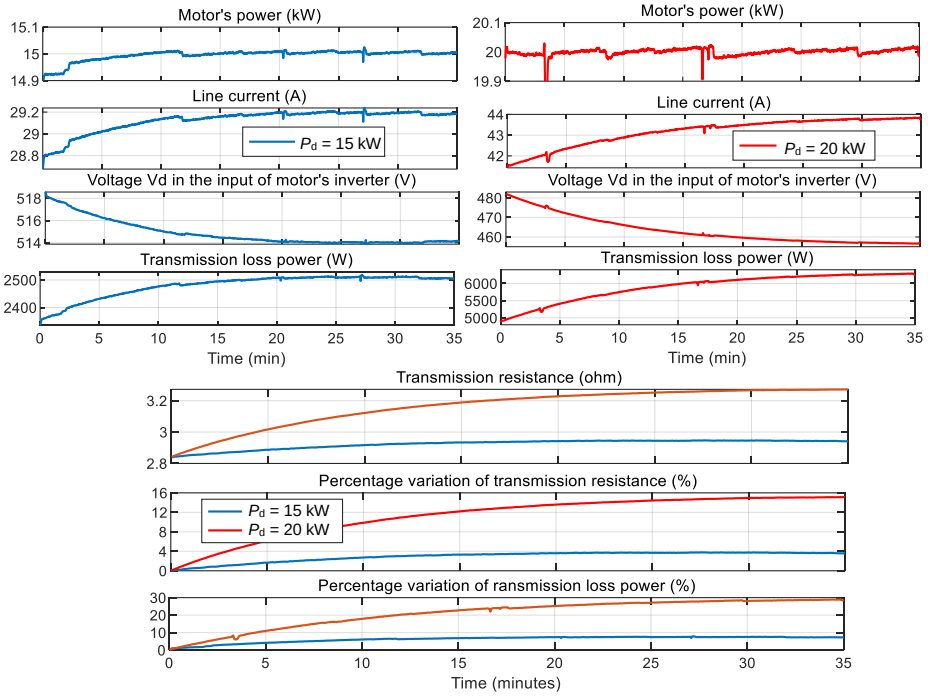

Fig. 2.18. Comparison of results for 15 kW and 20 kW at 400 m DC line length.

During experiments, the active rectifier voltage was the same as for the trolleybus substation, i.e. 600 V, but the 6 mm^2 wires had much smaller cross-sectional area and higher transmission resistance compared to the 100 mm^2 overhead wires. Hence, even at 15 kW and 20 kW, which are significantly lower than the trolleybus powers, there were significant voltage drops and losses. Therefore, when the power sources of stationary power consumers are located at long distances, it is recommended to select conductors with cross-sectional areas at which the transmission losses are as low as possible. In installations, the amount of transmission losses can be checked by measuring the consumer input voltage and comparing it with the power source voltage. If the difference is significant due to transmission losses, the existing wires should be either replaced with thicker ones or additional wires should be connected in parallel.

3. PLANNING OF ECONOMICAL MOBILE SUPERCAPACITOR ENERGY STORAGE SYSTEM FOR EFFICIENT USE OF REGENERATED ENERGY

A scaling method was developed for the design of mobile SC ESS, the purpose of which is not to ensure long autonomous driving distances but to store energy regenerated during trolleybus braking and use it during the next acceleration mode. The steps to be considered for scaling and planning such economical ESS are described hereafter.

Determining the amount of electric transport regenerated energy

The very first task in planning mobile SC ESS is to find out the energy amount that is regenerated by the vehicle under consideration, which in this case is trolleybus Škoda 27Tr, braking from the maximum permissible speed of 50 km/h till stopped. The simulations clarified that the actual regenerated energy is slightly lower than the corresponding kinetic energy due to various energy losses. Figure 3.1 shows the kinetic and regenerated energy for different loads of 27Tr. For further SC ESS planning actions, the passenger-filled 27Tr regenerated energy amount value was used because this is considered the maximum energy amount that the mobile SC ESS should be able to store.

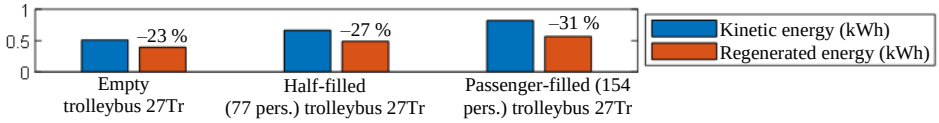

Fig. 3.1. Comparison of 27Tr kinetic and regenerated energies.

Calculating the necessary number of supercapacitor cells

The Maxwell 3 V 3400 F cells were chosen for prospective SC ESS planning. This cell model was released in January 2019 and is still the latest model in 2024 following the previous 2.7 V 3000 F and 2.8 V 3400 F cell models shown in Fig. 3.2.

Fig. 3.2. Cylindrical supercapacitor cell models.

To simplify the DC/DC converter topology, the minimum state-of-charge (SOC) voltage of ESS is usually set to half of the maximum SOC voltage, so the usable energy capacity of SC ESS is 75 % of its full energy capacity [26]. To determine the number of necessary SC cells, the regenerated energy amount must be compared with the usable energy capacities $E_{\mathrm{SC\_N}}$ for different combinations or numbers of SC cells which are calculated by the formula

$$E_{\mathrm{SC\_N}} = \frac{C_{\mathrm{N}}(V_{\mathrm{max\_N}}^2 - V_{\mathrm{min\_N}}^2)}{2}\left(\frac{1}{3600000}\right), \tag{3.1}$$

where

N – the number of SC cells, pieces;

C_N – total capacitance of circuit that contains N SC cells, F;
V_{max_N} – maximum permissible state-of-charge voltage of circuit with N SC cells, V;
V_{min_N} – minimum permissible state-of-charge voltage of circuit with N SC cells, V.

Nevertheless, during the lifetime of SC, their internal resistance R increases and their capacitance C or energy capacity decreases. It follows that if SC ESS is selected with initial energy capacity that is equal to the regenerated energy, the energy capacity will gradually decrease in time, with ESS being charged up faster and faster before the end of braking, thus dissipating more regenerated energy in brake resistors. Figure 3.3 shows the gradual decrease of C by 20 % and the gradual increase of R by 100 % over one million charge/discharge cycles.

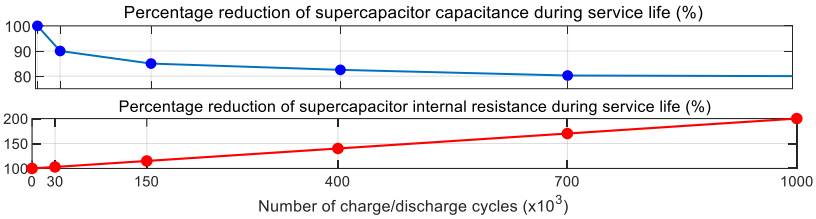

Fig. 3.3. Diagrams of supercapacitor parameter degradation over their lifetime.

It is worth noting that not all the regenerated energy E_r reaches the SC circuit as it first passes through the traction inverter and then through the ESS DC/DC converter. In both devices, some energy amount is lost. Even an ESS with an energy capacity that is exactly equal to the regenerated energy amount will not fully charge up at the start of exploitation. But after a certain period of use, its energy capacity will be decreased below the required amount. It was therefore recommended to plan SC ESS with an initial energy capacity E_{ESS} that is a certain amount higher than the maximum E_r that needs to be stored. Considering the traction drive inverter and DC/DC converter efficiencies η_{inv} un η_{con} and the decrease in energy capacity, the necessary E_{ESS} can be calculated by the following expression:

$$E_{ESS} = E_r + (nE_r - (1 - \eta_{inv}\eta_{con})E_r) = E_r(n + \eta_{tot}), \quad (3.2)$$

where n = 0.2 is the reduction (by 20 %) coefficient of the SC circuit energy capacity or capacitance and η_{tot} is the combined efficiency of traction drive inverter and DC/DC converter.

It is assumed that η_{inv} = 98 % and η_{con} = 98 %, $E_{EUS} \approx$ 0.66 kWh in (3.2). According to Fig. 3.4, where the necessary number of SC cells is determined, the E_{SC_N} curve that is calculated by (3.1) intersects with the E_{ESS} curve calculated by (3.2) at the number of 208 SC cells. Table 3.1 shows the parameters of SC ESS, and it was further assumed that this ESS consists of two series of 104 SC cells connected in parallel.

Table 3.1

Parameters of ESS with Energy Capacity 16 % Higher than Maximum Regenerated Energy

	N	V_{max} (V)	V_{min} (V)	C (F)	Active resistance (Ω)	Usable capacity (kWh)	Mass of SC cells (kg)	Full mass of ESS (kg)
27Tr *ESS*	208	312	156	65.38	0.01248	0.663	103	459

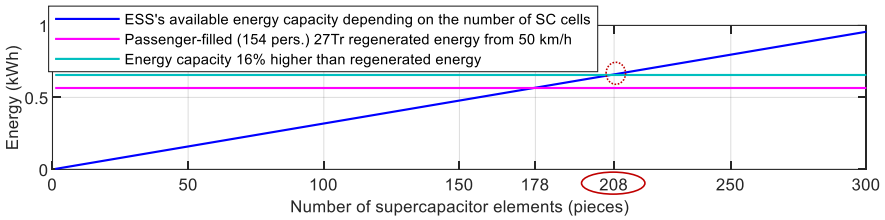

Fig. 3.4. Determination of the necessary number of SC cells for mobile ESS.

3.1. Efficiency of regenerated energy recovery

During the trolleybus braking, the regenerated energy E_r is delivered to SC ESS. However, during the charging process of SC, part of E_r is lost, as shown in Fig. 3.5, with E_r flow path to SC. The resistor R symbolizes the SC circuit internal resistance R. The E_{SC1} is the energy that reaches the SC circuit after passing through the drive inverter and the DC/DC converter:

$$E_{sc1} = E_r \eta_{inv} \eta_{dc/dc} = E_r \eta_{tot}. \quad (3.3)$$

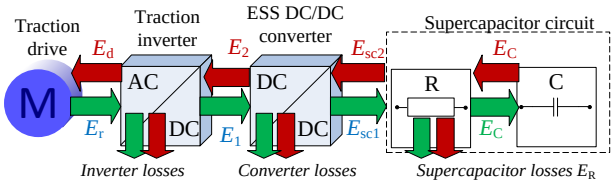

Fig. 3.5. Energy flow path during SC ESS charging and discharging modes.

A method to calculate E_R and E_C without performing simulations was developed. E_C must be calculated for calculating the charging process efficiency as the ratio between E_C and E_r:

$$\eta_{ch} = \frac{E_c}{E_r}. \quad (3.4)$$

Although the current is variable during the SC charging process, for approximate calculations, it can be assumed that the charging occurs at constant current I_{ch}, as shown in Fig. 3.6, where I_{ch} (red curve) corresponds to the average value of all actual current values (blue curve).

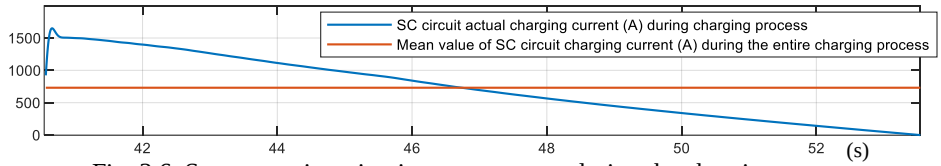

Fig. 3.6. Supercapacitor circuit current curves during the charging process.

Assuming that an SC circuit with capacitance C charges with constant current I_{ch} from initial voltage V_1 to voltage V_2 during time t, from general physics it is known that

$$I_{ch} = \frac{C(V_2 - V_1)}{t}. \quad (3.5)$$

I_{ch}, calculated by (3.5), and I_{ch}, calculated as the average of the sum of blue curve current values in Fig. 3.6 are practically equal within ± 1 % error. If the SC is charged from V_1 to V_2, then E_C can be substituted by the corresponding stored energy formula and E_R by the corresponding dissipated energy formula by using Expression (3.6).

$$E_{sc1} = E_c + E_R = \frac{C(V_2^2 - V_1^2)}{2} + \left(\frac{C(V_2 - V_1)}{t}\right)^2 Rt. \tag{3.6}$$

Simplifying (3.6) we obtain

$$E_{sc} = \frac{C\left((V_2^2 - V_1^2)t + (V_2 - V_1)^2 CR\right)}{2t}. \tag{3.7}$$

It can be checked if, in certain situations, the SC circuit is charged to the maximum voltage V_{max} by replacing V_2 with V_{max} = 312 V in (3.6) and (3.7). If $E_1 > E_{SC1}$, the SC circuit is charged to V_{max} because the difference between E_1 and E_{SC1} is the energy dissipated in brake resistors. If $E_1 < E_{SC1}$, the SC circuit is not charged to V_{max} and the V_2 calculation formula must be derived from (3.7) by obtaining a quadratic equation for calculating V_2:

$$C(t + 2CR)V_2 - 4C^2RV_1V_2 + 2C^2RV_1^2 - CtV_1^2 - 2E_{sc1}t = 0. \tag{3.8}$$

The root of (3.8) corresponding to the actual V_2 value has a (+) sign before the square root:

$$V_2 = \frac{4C^2RV_1 + \sqrt{(4C^2RV_1)^2 - 4C(t + 2CR)(2C^2RV_1^2 - CtV_1^2 - 2E_{sc1}t)}}{2C(t + 2CR)}. \tag{3.9}$$

In discharge, the energy discharged from SC is E_C. The energy E_d delivered to drive is

$$E_d = E_{sc2}\eta_{dc/dc}\eta_{inv} = E_{sc2}\eta_{tot}. \tag{3.10}$$

Discharge process efficiency can be calculated as E_d divided by E_C:

$$\eta_{dis} = \frac{E_d}{E_c}. \tag{3.11}$$

The formula of efficiency of E_r recovery of full SC charge/discharge process is

$$\eta_{ch/dis} = \frac{E_d}{E_r}. \tag{3.12}$$

Figure 3.7 on the left side shows the SC voltages at the end of charging mode for 27Tr braking from 50 km/h depending on the SC cell wear and the total efficiency of the traction drive inverter and DC/DC converter. The maximum ESS SC voltage V_{max} is not reached after the charging process, but in the example with the highest η_{tot} at the millionth charge/discharge cycle V_{max} is very close to the maximum voltage of 312 V. In the right side of Fig. 3.7 it is visible that the inverter and DC/DC converter efficiencies have significant impact on E_r recovery, so it is recommended to choose equipment with the highest possible η. Therefore, η_{inv} = 98 % and η_{con} = 98 % were assumed for the following calculations, resulting in η_{tot} = 96.04 %.

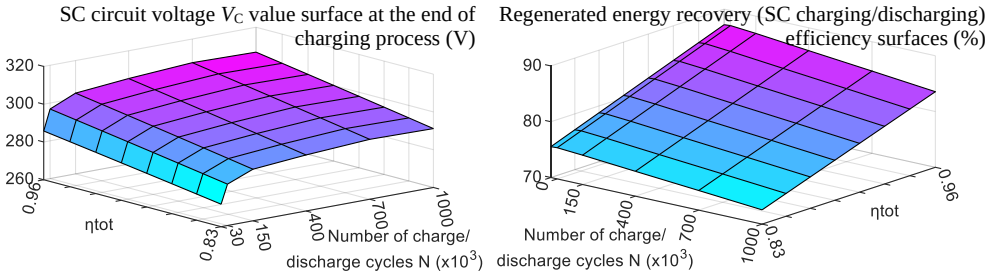

Fig. 3.7. SC circuit end-charging voltage and regenerated energy recovery efficiency surfaces.

3.2. Comparison of mobile supercapacitor ESS optimal discharge control strategies and their efficiencies

The study was based on 27Tr, which is half-filled with passengers and equipped with the previously calculated mobile ESS, accelerating to 50 km/h, as in Fig. 3.8. When braking from 50 km/h, 27Tr regenerates 0.493 kWh of which 0.458 kWh is successfully stored in ESS by charging it from 156 V to 273 V according to simulation results. Therefore, in each 27Tr acceleration simulation, the assumed initial ESS voltage was 273 V. 27Tr was located initially 1.5 km from the substation from which it moved away during motion. In the situation in Fig. 3.8, the ESS provides 50 % of the required power from the start of motion and discharges to minimum voltage about 2 seconds before the end of acceleration, thus causing the substation power peak. When the ESS is discharged, the drive voltage rapidly decreases due to the increase of overhead catenary voltage drop caused by the increase of current taken from the substation.

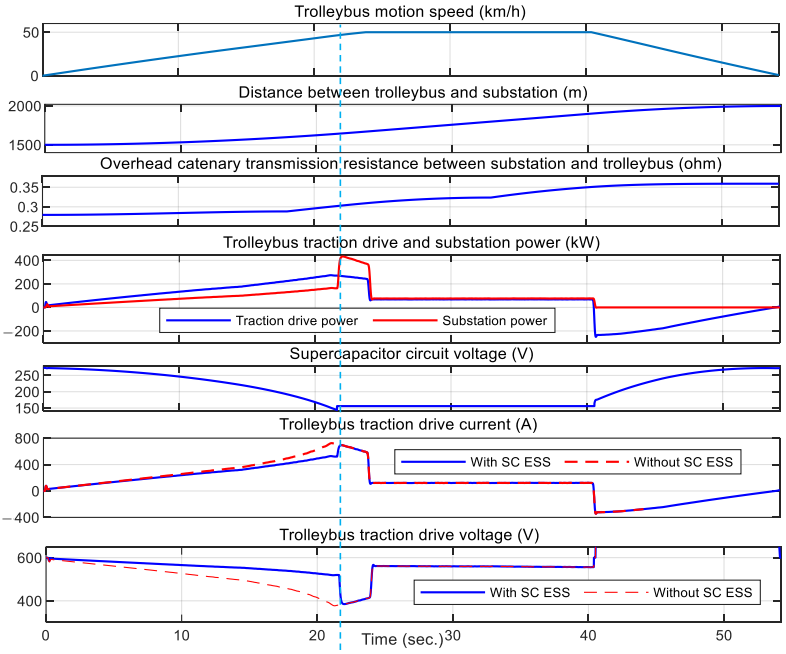

Fig. 3.8. Simulation results of 27Tr motion and its mobile SC ESS discharging/charging.

The applied ESS discharge strategies should actively involve the ESS in supplying power to the traction drive in the final part of the acceleration phase where the traction drive consumes more power. At higher powers taken from the substation, also transmission losses are correspondingly higher than, for example, at lower powers at the beginning of movement. If the ESS is able to contribute to the power supply at the end of acceleration, the substation's total energy consumption savings might be higher because they include not only the drive power portion that is provided by the ESS but also the avoided transmission losses and substation internal losses that would occur in the case of absence of ESS involvement.

SC discharging strategy with substation power peak shaving

From the trolleybus motion starting moment t_0 to the time t_1, only the substation provides the required power for the drive as shown in Fig. 3.9. At the time t_1 when the drive power reaches the value P_C, the SC ESS starts supplying the drive with power while constant power P_C is provided from the substation for the rest of acceleration mode till t_2. The intensity or proportionality k with which the SC ESS is discharged between t_1 and t_2 is calculated by

$$k = \frac{p_d - P_c}{p_d}. \tag{3.13}$$

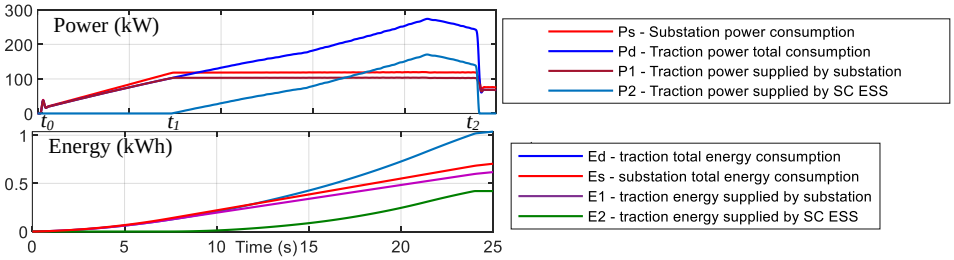

Fig. 3.9. Simulation results for SC discharging strategy with substation peak shaving.

SC discharging strategy with constant discharge proportionality

From the trolleybus motion starting moment t_0 until time t, the power required for the drive is provided by both the substation and the ESS with fixed distribution or proportionality, as shown in Fig. 3.10. The discharge proportionality corresponds to the coefficient k determining the drive power p_d portion that is provided by the ESS and calculated in real time by

$$p_2 = kp_d. \tag{3.14}$$

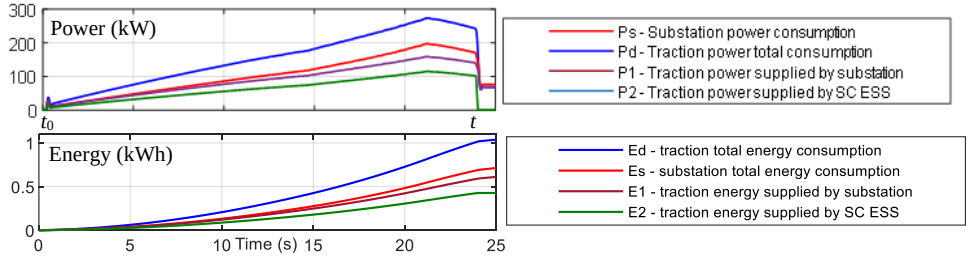

Fig. 3.10. Simulation results for discharging strategy with constant discharge proportionality.

Strategy with delayed SC discharging and constant discharge proportionality

From the trolleybus motion starting time t_0 until time t_1, only the substation provides the power required by the drive, as shown in Fig. 3.11. At the time t_1, when the drive power reaches a certain value P_a, the ESS starts supplying power as well. From t_1 to t_2, the drive is supplied by both the substation and the ESS with constant proportionality k.

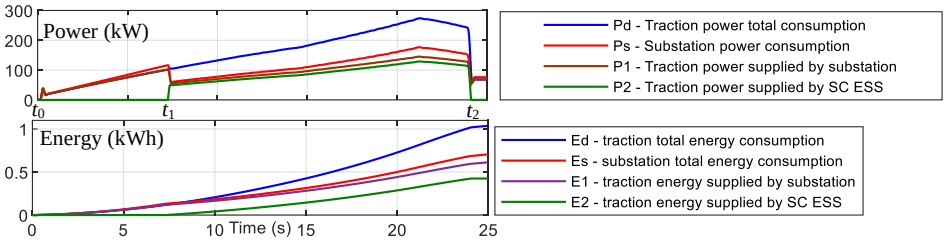

Fig. 3.11. Simulation results for SC discharging strategy with delayed discharge starting.

Comparison of efficiencies of SC discharging strategies

Hereafter, the situation in Fig. 3.8. is referred to as Strategy A, in Fig. 3.9 as Strategy B, in Fig. 3.10 as Strategy C, and in Fig .3.11 as Strategy D. During 27Tr acceleration, the ESS is discharged to a minimum voltage in all cases. Figure 3.12 shows that when ESS gets discharged till minimum in Case A, the substation energy consumption increases rather rapidly, resulting in this being the least efficient strategy compared to other ones which look nearly equivalent in terms of substation consumption curves nearly overlapping at the end of acceleration mode.

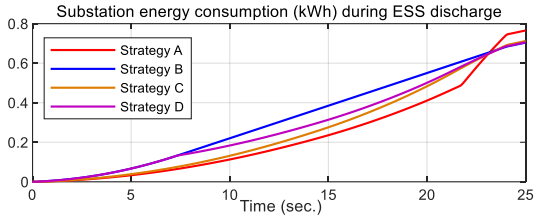

Fig. 3.12. Substation energy consumption curves for each considered SC discharging strategy.

The transmission loss curves in Fig. 3.13 make possible a more accurate strategy comparison concluding that in purely numerical terms, B is the most efficient strategy. In terms of transmission loss reduction, B is approximately 52 % more efficient than A. In terms of substation energy consumption reduction, of which transmission loss energy is a small part, B is 8 % more efficient than A. Strategies C and D are approximately 1 % less efficient than B.

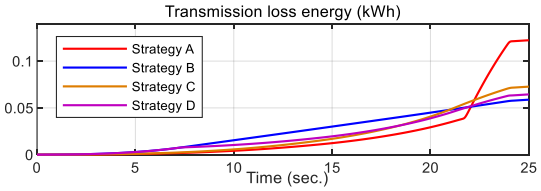

Fig. 3.13. Transmission loss energy curves for each considered SC discharging strategy.

3.3. Mobile supercapacitor ESS mass impact on transport vehicle energy consumption during motion

It should not be forgotten that equipping trolleybus with mobile ESS also increases its total weight meaning that the trolleybus becomes heavier and consumes more energy when moving. However, the extent to which the mobile ESS mass increases the drive energy consumption and whether this increase is significant compared to recoverable and usable regenerated energy has not been studied so far. It was therefore decided to investigate through simulations the mobile ESS mass impact not only on drive energy consumption during acceleration but also on substation total energy consumption in the case when the ESS exists but does not contribute to the drive power supply. For ESS mass calculation, the DC/DC converter mass was assumed to be $m_{\mathrm{dc/dc}}$ = 200 kg. The single SC cell mass is m_{sc} = 520 g, but per SC cell, there is an additional mass m_{d} = 750 g, which includes various busbars, balancing circuits, cooling systems, etc. The total mass of ESS is calculated by (3.15) where the number of SC cells N = 208:

$$m_{\mathrm{ESS}} = N(m_{\mathrm{sc}} + m_{\mathrm{d}}) + m_{\mathrm{dc/dc}}. \tag{3.15}$$

According to (3.15), the mobile SC ESS mass is 459 kg. Table 3.2 shows the percentage comparison of the total 27Tr masses without and with ESS for the cases of 27Tr being empty, half-filled, and fully filled with passengers. The ESS mass has the largest impact on 27Tr total mass in the case of empty 27Tr as here, the ESS mass makes a larger part of the total mass.

Table 3.2

Trolleybus 27Tr Masses

Empty trolleybus mass	19 000 kg
Empty trolleybus mass + ESS mass	19 459 kg (**+2.4 %**)
Half-filled trolleybus mass (77 passengers)	24 775 kg
Half-filled trolleybus mass + ESS mass	25 234 kg (**+1.9 %**)
Fully-filled trolleybus mass (154 passengers)	30 550 kg
Fully-filled trolleybus mass + ESS mass	31 009 kg (**+1.5 %**)

27Tr motion simulations with acceleration from a standstill to 50 km/h in 23.8 seconds were made. Due to the additional mass of ESS, the transmission loss energy increases above 5 % in all cases, according to Fig. 3.14, but the substation energy consumption increase is less than 3.5 % in all cases since the transmission loss energy is a relatively smaller part of the substation energy consumption. Moreover, the transmission loss and substation energy differences shown in Fig. 3.14 are actual only when the ESS is placed on board of 27Tr but is switched off. If the mobile ESS does not function, then it just travels with the trolleybus as a parasitic mass.

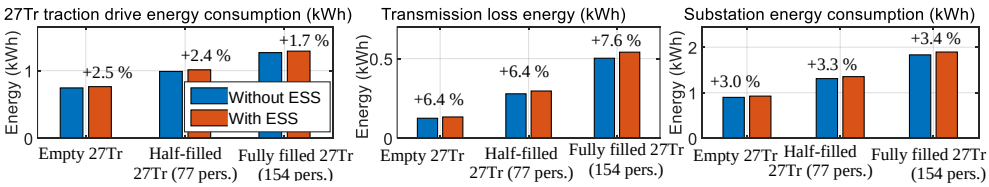

Fig.3.14. Energy consumption when 27Tr accelerates to 50 km/h with and without ESS mass.

Figure 3.15 shows the power curves of half-filled 27Tr when it is initially 1.5 km from the substation and accelerates to 50 km/h for the cases with ESS (discharge strategy C) and without ESS. The ESS application significantly reduces the substation's total power consumption. The area limited by the substation power consumption in the case without ESS (yellow line) and the substation power consumption in the case with functioning ESS (green line) can be considered as saved substation energy amount being approximately 48 % in the current situation. It can be concluded that when the ESS is applied, the substation energy savings simply outweigh the mobile ESS's main disadvantage related to the trolleybus mass increasing.

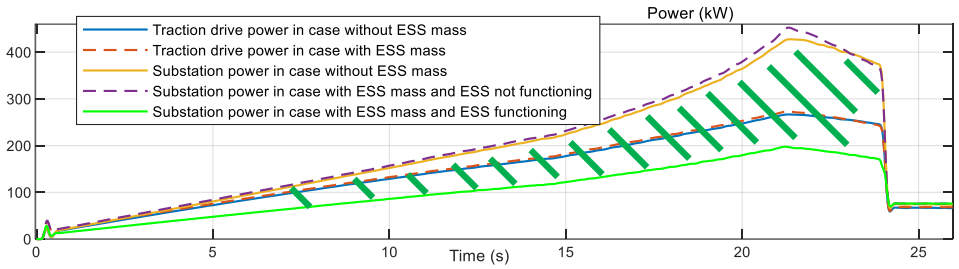

Fig. 3.15. Comparison of power curves for situations with and without mobile SC ESS.

3.4. Calculation of financial savings achieved by using mobile supercapacitor ESS

The beginning phase of mobile SC ESS implementation can be considered as a payback period, which lasts until the amount of successfully recovered energy is equal in financial terms to the ESS purchase and installation cost. After this period, it can be claimed that the ESS indirectly makes a profit at the expense of the recovered energy cost that would have to be paid in the absence of ESS. A proposal was made on how to approximate the full amount of energy that ESS can store during its lifetime, i.e. being charged/discharged until its capacitance C has decreased by 20 % and its internal resistance R has increased by 100 %.

The calculation of ESS profit described further was based on fully filled 27Tr accelerating up to 50 km/h and braking for one million times, which is the number of times the SC cell can be charged/discharged during its service life. According to the manufacturer, this number of 10^6 charge/discharge cycles refers to full charge/discharge, but it should be noted that in the trolleybus case, the mobile SC ESS minimum voltage is half of the maximum voltage. Also, the operating temperature of mobile ESS can exceed the nominal 25 °C, thus causing faster wear of SC cells. Therefore, its charging from $V_{min} = 0.5V_{max}$ to V_{max} and discharging from V_{max} to $V_{min} = 0.5V_{max}$ was considered as full charge/discharge cycle.

Approximate calculation of trolleybus recovered energy during SC service life

Simulations showed that a fully filled 27Tr regenerates approximately 0.562 kWh of energy during one braking operation. Therefore, such 27Tr recovers 562 000 kWh of energy in one million times. Assuming that the price per kWh is, for example, 0.15 EUR, the calculated cost of recovered energy corresponds to 84 300 EUR. This amount is sufficient to consider the use

of mobile SC ESS. It is understandable that the actual price of saved energy is going to be lower than this amount due to regenerated energy losses in the inverter, DC/DC converter and due to SC internal resistance. Therefore, the next step is to calculate the cost of the regenerated energy part that is successfully used for accelerating the 27Tr traction drive during the whole SC ESS lifetime.

Figure 3.16 shows the plot of the total 27Tr energy regenerated from 50 km/h (blue) till stopping, the regenerated energy portion successfully stored (red), and the regenerated energy portion successfully used during accelerations modes that follow braking modes from the first till the millionth charge/discharge cycle. The green curve can be used to calculate the total energy that is successfully recovered and used by the traction drive over the ESS lifetime since this energy area corresponds to the plane area marked by thicker green lines and bordered by the green regenerated energy line from above. The calculation is performed using the trapezoidal method. The area of successfully recovered energy is divided into five trapezoids, for each of which the areas are calculated separately and then summed. For example, the area S_3 is calculated using the expression for trapezoidal area:

$$S_3 = E_{ESS\_S3(kWh)} = \left(\frac{ab + cd}{2}\right) ad, \tag{3.16}$$

where

ab – successfully recovered energy at the 150 000th cycle, kWh;

dc – successfully recovered energy at the 400 000th cycle, kWh;

ad – number of cycles between the 150 000th and 400 000th cycle, cycles.

The areas of all the other trapezoids are calculated in the same way. The total recovered energy is calculated as the sum of the areas of corresponding trapezoids:

$$E_{ESS} = S_1 + S_2 + S_3 + S_4 + S_5 \tag{3.17}$$

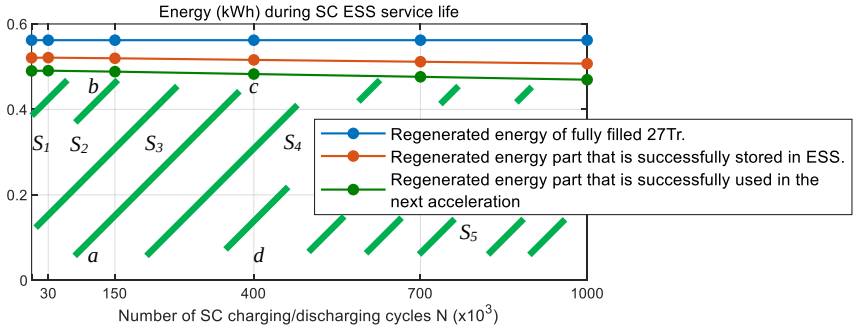

Fig. 3.16. Curves of stored and used regenerated energy during mobile SC ESS lifetime.

According to calculation results, the total amount of regenerated energy successfully used during ESS lifetime is E_{ESS} = 514 434 kWh, which is considered as an “indirect” drive energy consumption saving that would otherwise be consumed from the substation in the absence of mobile SC ESS.

Calculation of the estimated profit to be achieved from the use of supercapacitors

Expenses which are related to mobile ESS purchase and installation cost are recovered when the cost of regenerated energy that has been successfully used since the beginning of ESS exploitation is equal to the ESS purchase and installation cost which can be calculated by

$$K_{\text{ESS}} = NK_{\text{SC}}k, \tag{3.18}$$

where

N – the number of SC cells, pieces;

K_{SC} – the cost of one SC cell, €;

$k = 2$ – the coefficient of the DC/DC converter and SC installation cost [27], [28].

The energy consumption saving in financial terms over the entire lifetime of ESS considering only the energy that is regenerated by traction drive can be calculated by

$$K_{\text{d}} = E_{\text{ESS}}K_{\text{kWh}} - K_{\text{ESS}}, \tag{3.19}$$

where E_{ESS} is the amount of regenerated energy successfully used during SC lifetime, kWh, and K_{kwh} is electrical energy cost per kWh, €.

However, (3.19) does not yet calculate the cost of the substation's total saved energy, which includes not only the regenerated energy E_{ESS} but also the decrease of transmission losses and the decrease of substation internal losses due to less power taken from the substation. To estimate the substation's total energy consumption saving K_{s} over the entire lifetime of ESS, it was proposed to first simulate the motion of fully filled 27Tr without mobile ESS, register the substation energy consumption at the end of acceleration, and then simulate the motion of fully filled 27Tr equipped with a functioning mobile ESS and register the substation energy consumption at the end of acceleration. The difference in consumptions between the first and the second case is E_{S} and the financial value K_{s} over the ESS lifetime can be calculated by considering also the ESS purchasing and installation cost according to (3.20):

$$K_{\text{s}} = E_{\text{s}}K_{\text{kWh}} - K_{\text{ESS}}. \tag{3.20}$$

For approximate calculations, 1 km was assumed as the average distance between the substation and trolleybus and the motion of a passenger-filled 27Tr was simulated. Figure 3.17 shows simulation results for situations without and with mobile ESS discharged according to the constant discharging proportionality strategy. The difference in substation energy consumption between the two cases is 0.7066 kWh. Therefore, to obtain the E_{S} value over the entire ESS lifetime, this number must be multiplied by 10^6. Then E_{S} = 706 600 kWh, which is higher compared to the total successfully used regenerated energy E_{ESS} = 514 434 kWh.

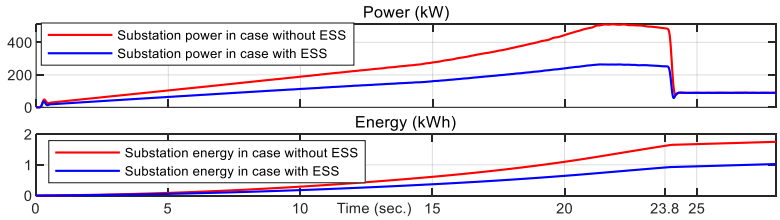

Fig. 3.17. Simulation results of substation power and energy consumption.

The previously called “indirect” profits on the expense of energy savings due to ESS use were further calculated assuming that the price of electricity per kWh might vary between 0.1 euro and 0.18 euro but the potential price per SC cell might vary between 46 euro and 62 euro. In this case, the profit is not meant as a direct financial income but as a decrease of the cost shown in electricity bills. Since the SC cell and electricity prices were set as variables, three dimensional surfaces were obtained. Figure 3.18 on the left side shows the profit amount surface considering only successfully used regenerated energy while the right side shows the profit mount surface considering the substation’s total energy consumption, and it is visible that in the second case, the profits are higher.

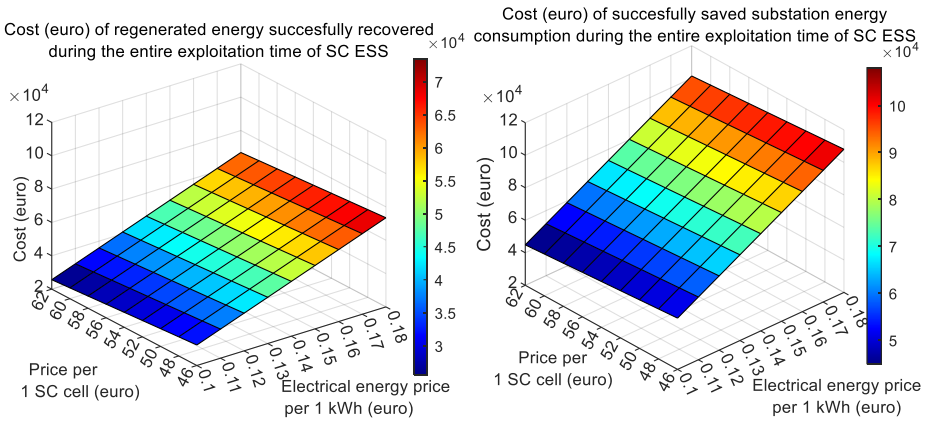

Fig. 3.18. Energy savings in financial terms due to the mobile ESS use.

Also, looking at the price difference comparison in Fig. 3.18, it can be concluded that the financial savings are more significant if the estimations consider substation energy savings E_S rather than only the regenerated energy E_{ESS}. The percentage difference between E_S and E_{ESS} prices is higher at lower electricity prices and higher SC cell of ESS purchase/installation costs. In Fig. 3.19, it can be seen that the financial return of ESS is affected by the electricity price significantly more than the total price of ESS. It follows that applying mobile SC ESS can be financially beneficial in the case of electricity price inflation. However, when the electricity price decreases, the ESS payback period will be longer, and the resulting financial return or indirect profit will be lower due to the lower price of the saved energy.

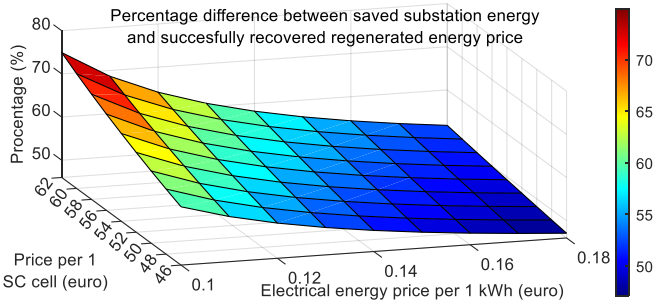

Fig. 3.19. Difference between the prices of saved substation energy and regenerated energy.

4. EFFICIENCY COMPARISON OF SUPERCAPACITOR CONSTANT CURRENT AND CONSTANT POWER CHARGING/DISCHARGING

For the calculation, design and modelling of a large-scale SC ESS, the RC circuit (resistor-capacitor) model is most used as an equivalent replacement of a real SC circuit [29].

The efficiencies for constant-current charging and constant-power charging, the efficiencies for constant-current discharging and constant-power discharging, as well as the total charging/discharging efficiencies of both methods, were compared by calculations and simulations based on the RC model. The study was based on an SC circuit consisting of twenty series-connected SC cells Maxwell BCAP0450 P270 S18, shown in Fig. 4.1. According to the manufacturer's information, single SC cell's C = 450 F, R = 2.8 mΩ, and maximum voltage V_C = 2.7 V. Hence, for twenty SC cells in series, C = 22.5 F, R = 0.056 Ω and V_C = 54 V.

Fig. 4.1. Supercapacitor series-connection circuit.

In charging cases, the SC circuit was charged from initial voltage V_{C1} = 27 V to final voltage V_{C2} = 54 V within time t = 25 s. In following discharging cases, the SC circuit was discharged from initial voltage V_{C1} = 54 V to final voltage V_{C2} = 27 V within time t = 25 s.

Constant-current charging/discharging

Figure 4.2 shows the charging and discharging of the RC circuit equivalent to the SC circuit, where the constant parameters, such as current I_C, are denoted by capital letters and the variable parameters by small letters. In charging, the I_C flows towards C, so the potentials on R and C are in equal directions, while in discharging, the I_C flows away from C, so the potentials on R and C are in opposite directions. The voltage v_c is the internal or actual voltage of the SC circuit, while the resistance R-caused voltage drop V_R is constant due to constant I_C.

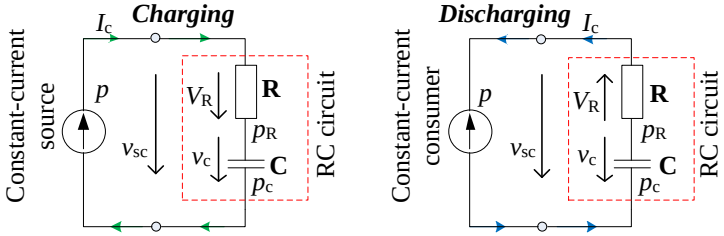

Fig. 4.2. Depiction of SC circuit charging and discharging processes in equivalent RC circuit.

SC circuit external voltage v_{SC} indicated by the voltmeter during charging mode is

$$v_{SC} = v_C + V_R = v_C + I_C R. \tag{4.1}$$

SC circuit external voltage v_{SC} indicated by the voltmeter during discharging mode is

$$v_{SC} = v_C - V_R = v_C - I_C R. \tag{4.2}$$

From (4.1) and (4.2), it follows that in charging mode, the voltage v_{SC} indicated by the voltmeter is higher than v_C, but in the discharging mode, it is lower. As soon as charging or discharging stops, the voltmeter immediately indicates the voltage value V_C. The constant current for charging the SC circuit from initial voltage V_{C1} to final V_{C2} in a certain time t is

$$I_C = \frac{C(V_{C2} - V_{C1})}{t}. \tag{4.3}$$

The discharge current is also calculated by (4.3). If charging and discharging occur at equal time periods and voltage ranges, the currents in both modes are equal but with opposite flow directions. The discharging efficiency is the product of successfully stored energy E_{C1} divided by the total energy E_{SC1} fed to the SC circuit. E_{SC1} consists of E_{C1} and energy E_{R1} lost due to R:

$$\eta_{ch} = \frac{E_{C1}}{E_{SC1}} = \frac{E_{C1}}{E_{C1} + E_{R1}} = \frac{C(V_{C2}^2 - V_{C1}^2)}{C(V_{C2}^2 - V_{C1}^2) + 2I_C^2 Rt}. \tag{4.4}$$

The successfully discharged energy E_{SC2} is the difference between the total discharged energy E_{C2} and the lost energy E_{R2}. The discharge efficiency is the ratio of E_{SC2} and E_{C2}:

$$\eta_{dis} = \frac{E_{SC2}}{E_{C2}} = \frac{E_{C2} - E_{R2}}{E_{C2}} = \frac{C(V_{C2}^2 - V_{C1}^2) - 2I_C^2 Rt}{C(V_{C2}^2 - V_{C1}^2)}. \tag{4.5}$$

The total efficiency of the charging/discharging process, when charging from V_{C1} to V_{C2} and discharging from V_{C2} to V_{C1} occur at equal times, can be calculated as the successfully discharged energy E_{SC2} divided by the total energy E_{SC1} fed to the SC circuit in charging mode.

$$\eta_{ch/dis} = \frac{E_{SC2}}{E_{SC1}} = \frac{E_{C2} - E_{R2}}{E_{C1} + E_{R1}} = \frac{C(V_{C2}^2 - V_{C1}^2) - 2I_C^2 Rt}{C(V_{C2}^2 - V_{C1}^2) + 2I_C^2 Rt}. \tag{4.6}$$

Constant-power charging/discharging

In charging mode, the constant parameter is the supplied power P. In discharging mode, the constant parameter is the successfully discharged power P. Other parameters like charge/ discharge current i_C, voltage drop v_R, and internal voltage v_C are variables as shown in Fig. 4.3.

In charging, the constant supplied power P is equal to the sum of the successfully stored power p_C and the power losses p_R:

$$P = p_C + p_R = i_c v_c + i_c^2 R. \tag{4.7}$$

During charging, the following relationship exists between current i_C and capacitance C:

$$v_C'(t) = \frac{i_C}{C}. \tag{4.8}$$

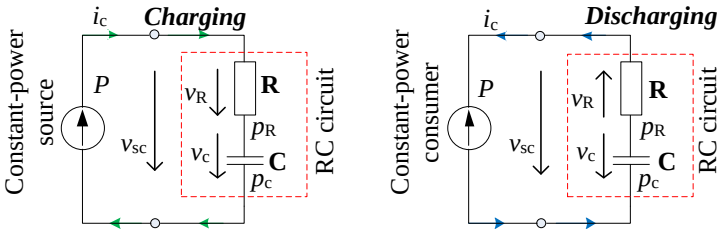

Fig. 4.3. Depiction of SC circuit charging and discharging processes in equivalent RC circuit.

Using (4.8) to transform Equation (4.7), the following differential equation is obtained:

$$RC^2 v'_{\mathrm{C}}(t)^2 + C v_{\mathrm{C}} v'_{\mathrm{C}}(t) - P = 0. \tag{4.9}$$

Dividing (4.9) by C results in quadratic Equation (4.10), the correct root of which is (4.11):

$$RC v'_{\mathrm{C}}(t)^2 + v_{\mathrm{C}} v'_{\mathrm{C}}(t) - \frac{P}{C} = 0, \tag{4.10}$$

$$v'_{\mathrm{C}}(t) = \frac{-v_{\mathrm{C}} + \sqrt{v_{\mathrm{C}}^2 + 4RP}}{2RC}. \tag{4.11}$$

From (4.11), the differential Equation (4.12) can be derived and integrated to obtain the charging time t calculation formula (4.13) if v_{C} varies from V_{C1} to V_{C2} during t:

$$dt = \frac{2RC}{-v_{\mathrm{C}} + \sqrt{v_{\mathrm{C}}^2 + 4RP}} dv_{\mathrm{C}}, \tag{4.12}$$

$$t = \frac{C}{4P}\left(V_{\mathrm{C2}}^2 - V_{\mathrm{C1}}^2 + V_{\mathrm{C2}} \cdot \sqrt{4RP + V_{\mathrm{C2}}^2} - V_{\mathrm{C1}} \cdot \sqrt{4RP + V_{\mathrm{C1}}^2} + 4RP \cdot \mathrm{LN}\left(\frac{V_{\mathrm{C2}} + \sqrt{4RP + V_{\mathrm{C2}}^2}}{V_{\mathrm{C1}} + \sqrt{4RP + V_{\mathrm{C1}}^2}}\right)\right). \tag{4.13}$$

From (4.13), no formula for P at known t can be derived. An option to find P values is to obtain the table of Equation (4.13) solutions for various P values, thus allowing to search for the P value for certain t as shown in Fig. 4.4. In this example, t values are calculated at P ranging from 750 W to 9000 W with the changing step of 0.1 W due to which certain errors in the calculation might take place. To reduce the error, the changing step should be even smaller. For example, searching for P at time t = 25 s, the closest found actual value of t obtained by (4.13) is approximately 25.0012 s, as shown in Fig. 4.4. This error representing a thousandth of a second is negligible, so the corresponding P = 1018.3 W can be selected for further calculations.

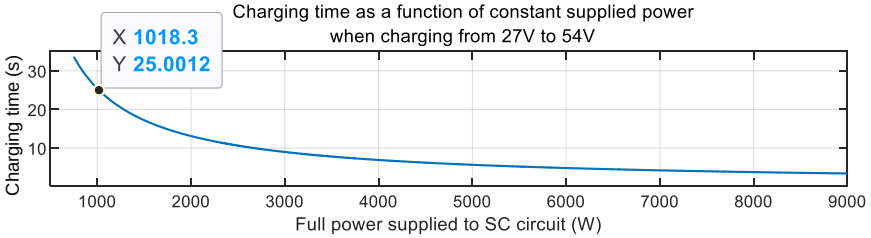

Fig. 4.4. The diagram of SC charging time vs constant supplied power.

In discharging, the consumer that is connected to the SC circuit consumes constant power P corresponding to the difference between the total discharged power p_C and the lost power p_R:

$$P = p_C - p_R = v_C i_C - i_C^2 R. \tag{4.14}$$

During discharging, the following relationship exists between current i_C and capacitance C:

$$v'_C(t) = -\frac{i_C}{C}. \tag{4.15}$$

Using (4.15) to transform Equation (4.14), the following differential equation is obtained:

$$RC^2 v'_C(t)^2 + C v_C v'_C(t) + P = 0. \tag{4.16}$$

Dividing (4.16) by RC^2 results in quadratic Equation (4.17) with the correct root of (4.18):

$$v'_C(t)^2 + \frac{v_C}{RC} v'_C(t) + \frac{P}{RC^2} = 0, \tag{4.17}$$

$$v'_C(t) = \frac{-v_C \pm \sqrt{v_C^2 - 4PR}}{2RC}. \tag{4.18}$$

From (4.18) the differential Equation (4.19) can be derived and integrated to obtain the discharging time t calculation formula (4.20) if v_C varies from V_{C2} to V_{C1} during t [30]:

$$dt = \frac{2RC}{-v_C + \sqrt{v_C^2 - 4PR}} dv_C, \tag{4.19}$$

$$t = \frac{C}{4P}\left(V_{C2}^2 - V_{C1}^2 + V_{C2} \cdot \sqrt{V_{C2}^2 - 4PR} - V_{C1} \cdot \sqrt{V_{C1}^2 - 4PR} - 4PR \cdot \mathrm{LN}\left(\frac{V_{C2} + \sqrt{V_{C2}^2 - 4PR}}{V_{C1} + \sqrt{V_{C1}^2 - 4PR}}\right)\right). \tag{4.20}$$

For the discharge process, either only time t or only power P can be equal to the corresponding charging process parameter. If the discharging and charging processes are decided to have equal durations t, then the constant power consumed during discharging is less than the constant power during charging. For charging occurring from 27 V to 54 V and discharging from 54 V to 27 V, Fig. 4.5 shows in one plane the time comparison of charging and discharging processes versus constant charge/discharge power. With increasing power and decreasing comparative charge/discharge time t, the difference between the charge and discharge durations increases.

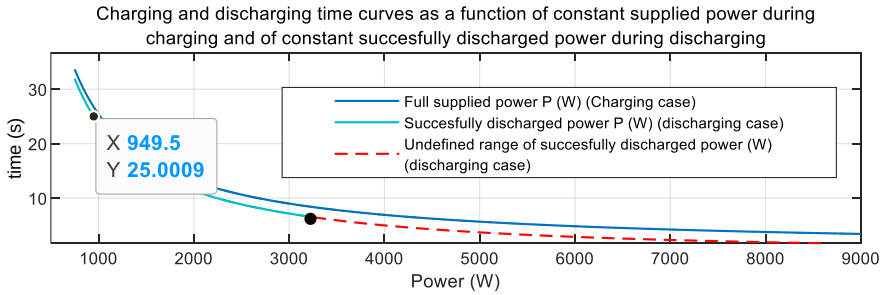

Fig. 4.5. Diagrams of SC charging and discharging times vs constant supplied/consumed power.

In Fig. 4.5, the green curve becomes red at one point (3254.5 W) meaning that for further powers of P in (4.20), the values of sub-root expressions that contain V_{C2} turn negative. The red dashed curve corresponds to real parts of complex numbers of the (4.20) solutions, but in general, it is an undefined region of power values at given discharge time conditions, i.e. it is not possible to discharge the SC circuit from 54 V to 27 V with these power values.

The total efficiency of charging/discharging is calculated similarly as by (4.4), (4.5), and (4.6). In this case, the successfully discharged energy is the product of power P and time t:

$$E_s = Pt. \tag{4.21}$$

4.1. Comparison of SC circuit constant-current and constant-power charging and discharging efficiency results

Figure 4.6 shows SC circuit charging and discharging simulation results of 25-second long charging from 27 V to 54 V and 25-second long discharging from 54 V to 27 V. Figure 4.7 shows the real-time variation of power-storing efficiency and energy-storing efficiency.

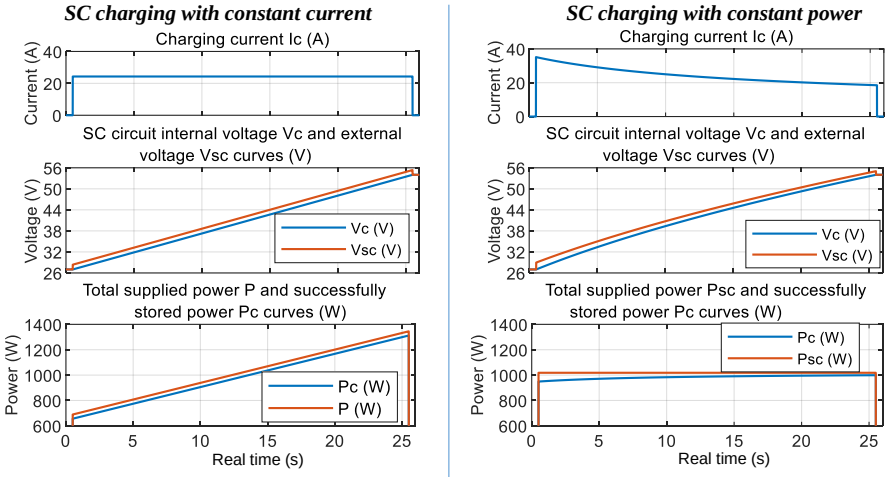

Fig. 4.6. SC circuit constant-current and constant-power charging simulation results.

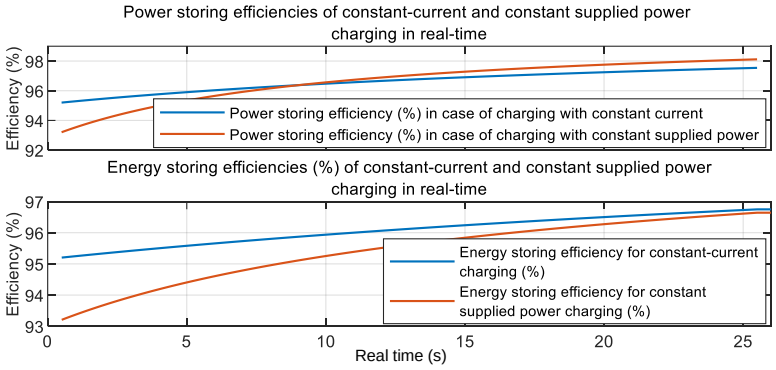

Fig. 4.7. Comparison of power and energy storing efficiency in real time.

The total energy storage efficiency of the entire charging process corresponds to the value at the end of the charging process, and Fig. 4.7 shows that this value is higher for the constant charging current method than for the constant supplied power method. Figure 4.8 shows that also the total energy discharging efficiency at the end of the discharging process is higher for the constant-current method than for the constant successfully discharged power method.

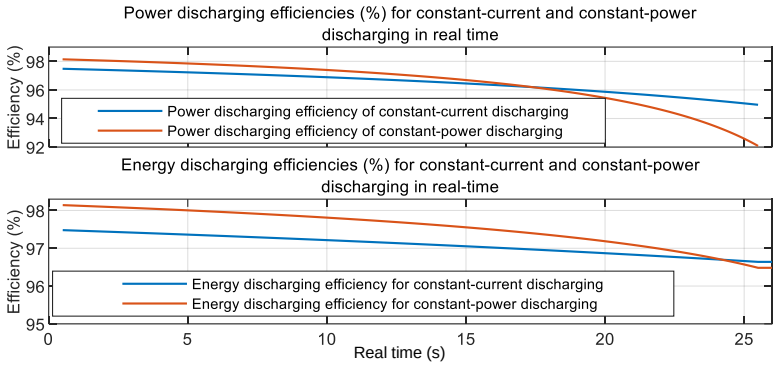

Fig. 4.8. Comparison of power and energy discharging efficiency in real time.

It was decided to compare charging processes lasting 4–30 s (with a 1 s changing step) and following discharging processes lasting the same amount of time. The maximum recommended peak current of the given SC cells is 240 A, so 1–3 s charging and/or discharging were not considered. The results in Fig. 4.9 show that the SC charging with constant current is more efficient than charging with constant power all the time and the difference in these conditions is 0.1–0.25 %, being larger for faster charging and lower for longer charging.

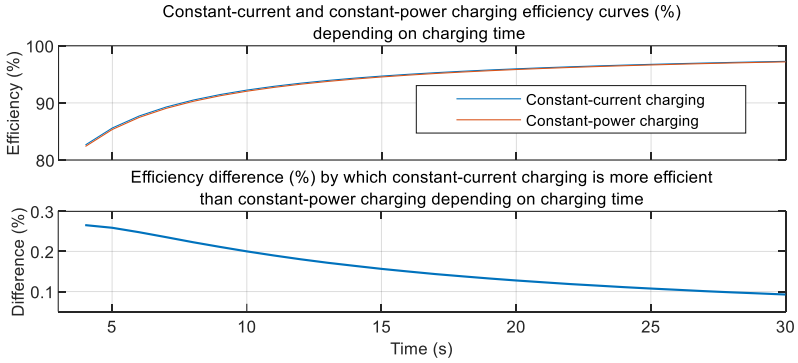

Fig. 4.9. Comparison of charging efficiencies depending on the charging time.

The minimum time for a constant-power discharge is 7 s because, at lower values, the sub-root expressions with V_{C2} in (4.20) are negative. So, for charging faster than 7 s, there is no valid constant power. Figure 4.10 shows that SC discharging with constant current is more efficient than SC discharging with constant power, and the difference in the given conditions is 0.12–1 %, which is more noticeable compared to the charging case differences.

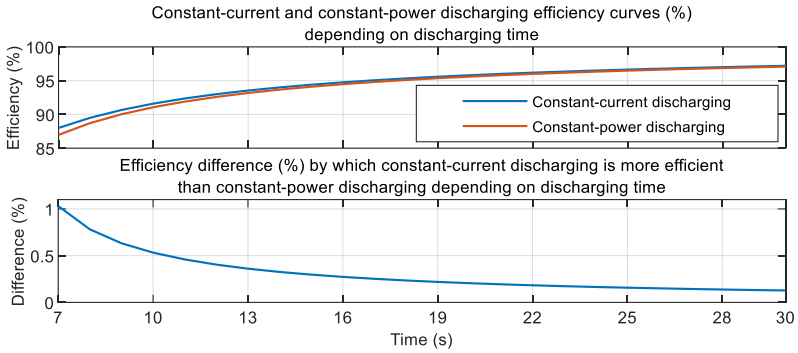

Fig. 4.10. Comparison of discharging efficiencies depending on the discharging time.

Fig. 4.11 shows that the total charging/discharging efficiency is higher for the constant-current method than for the constant-power method. The percentage difference is 0.2–1.1%, being higher for faster charging/discharging processes and lower for longer charging/discharging processes.

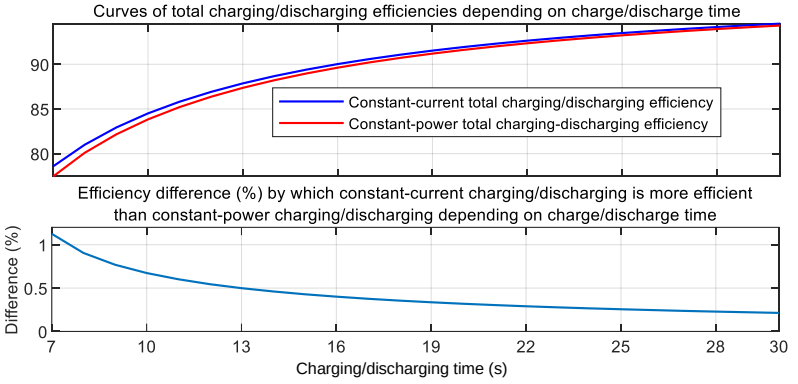

Fig.4.11. Comparison of total charging/discharging process efficiencies depending on charging and discharging time.

The differences between the constant-current charging being more efficient than the constant-power charging and the differences between the constant-current discharging being more efficient than the constant-power discharging were tested depending on the variation of SC circuit internal resistance R that might reach approximately 0.14 Ω for the given SC circuit after 10^6 charge/discharge cycles. Therefore, difference comparisons were performed for the case where the same SC circuit is charged from 27 V to 54 V in 25 s at different R from 0 Ω to 0.14 Ω with a changing step of 0.004 Ω. According to calculations, charging and discharging with constant current is more efficient anyway, except when there is no internal resistance, i.e. R = 0 Ω because then both strategies are 100 % efficient, but such a case is impossible as any capacitor has a certain resistance. According to Fig. 4.12, at lower R, the difference between the charging/discharging processes is lower, while at higher R, the difference gradually increases.

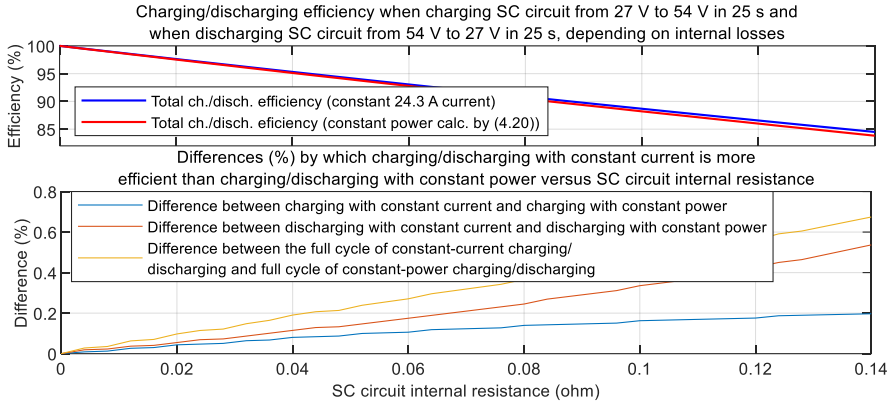

Fig. 4.12. The charging/discharging efficiency comparison depending on the SC resistance.

The discovered difference in efficiencies being below 1% reveals that the constant-current charging/discharging is insignificantly more efficient than the constant-power charging/discharging. Therefore, both methods might be considered as nearly equivalent. Nevertheless, the performed calculations and simulation results have fundamental theoretical value since they prove and justify that as far as the RC model is considered, capacitor charging with constant current is not identical to charging with constant power and capacitor discharging with constant current is not identical to discharging with constant power in terms of efficiency.

4.2. Experimental charging/discharging of SC circuit and comparison of measurements with simulation results

In addition to calculations and simulations based on the RC circuit model, it was decided to perform charging/discharging on a real SC circuit to check whether the theoretical reasoning that constant-current charging/discharging is more efficient than constant-power charging/discharging can be verified in practice if the difference is very low, i.e. below 1 %.

The same SC circuit (Fig. 4.1) was charged using a laboratory power source and discharged using an electronic load. The SC circuit's initial minimum voltage was $V_{C1} = 27$ V and the final voltage was $V_{C2} = 50$ V. Charging and discharging time durations were 30 s each. Measurements were made using the bench (see Fig. 4.13) and compared with simulation results. However, when calculating using an RC circuit, the parameter R should not only consider the SC circuit's internal resistance because the circuit board conductive traces might also have certain significant resistance. Micro ohmmeter indicated 46 mΩ resistance of the traces.

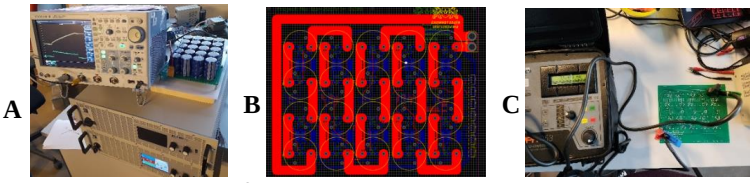

Fig. 4.13. A – a bench for measuring, B – conductive traces, C – trace resistance measuring.

For 30 s discharging and charging, the constant charge/discharge current is 17.25 A by (4.1), the constant supplied charging power is 697.1 W by (4.13), and the constant consumed power for discharging is 630.6 W by (4.20). Figure 4.14 shows the measurement and simulation results, and some differences are visible. One reason for the inaccuracies is the use of a simplified RC model for calculations and simulations; the other is that SC circuit capacitance C might differ from the calculated one as C decreases in time, and SC internal resistance R might differ as R increases in time. In addition, the C and R of individual SC elements might have changed unevenly as the voltage balancing circuit might not provide equal voltages to the SC elements. Therefore, before and after charging/discharging, the voltages on each SC element were measured to check how evenly the circuit voltage was distributed. Some voltage shifts were found, as visible in Fig. 4.15, with some kind of symmetry of shifts for each of the four following SC elements. The maximum differences are between 0.04 V and 0.06 V.

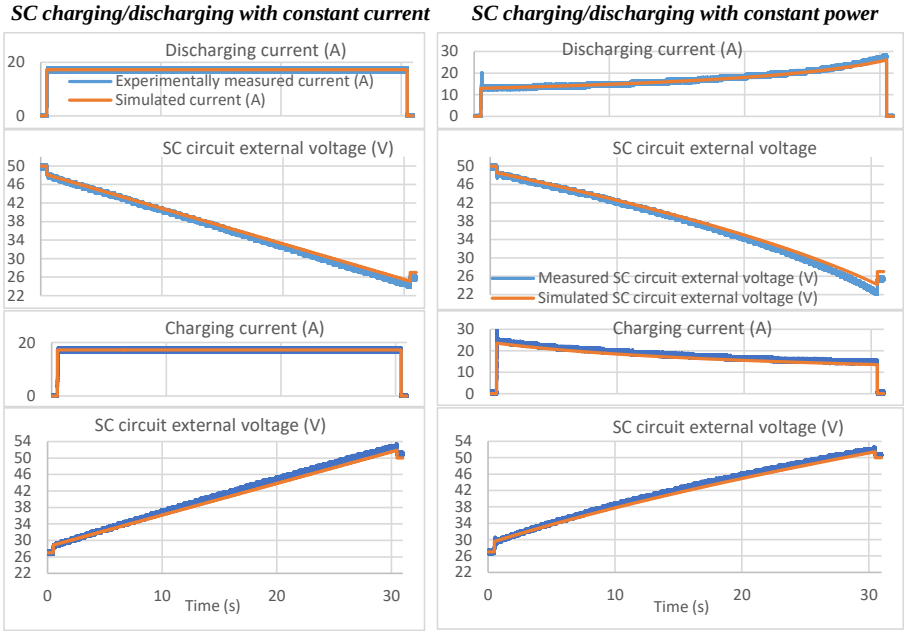

Fig. 4.14. Comparison of SC circuit discharging/charging measurements and simulation results.

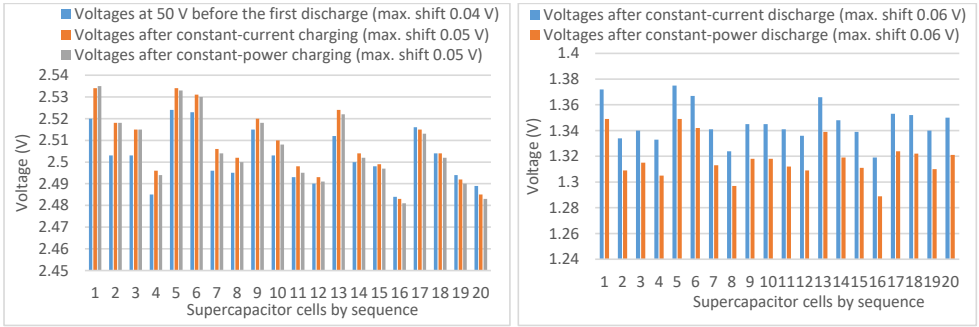

Fig. 4.15. Voltage values for each SC cell.

5. CONCLUSIONS

Since overhead grid-connected electric public transport infrastructure is one of the largest electricity consumers, improving the energy efficiency of this infrastructure by reducing electrical energy consumption is a topical issue. During braking mode, regenerative drives in electric vehicles such as trolleybuses regenerate braking energy, which can be stored in mobile SC ESS and used during the next acceleration as the main way to reduce the total electrical energy consumption. This purpose requires the design of an economical mobile SC ESS that is designed for the storage and use of regenerated energy but not for providing long autonomous distances. However, the initial energy capacity of such ESS should be by a certain reserve amount higher than the regenerated energy that must be stored since the SC energy capacity decreases gradually over its operation time. The use of SC ESS also prevents potential transmission losses, which would occur if the power to the trolleybus drive flew only from a substation. Therefore, there is a need for tools or computer models to simulate trolleybus motion to study whether the use of SC ESS would be effective in certain situations, considering the amount of saved energy, which also includes prevented transmission losses. For this purpose, three options were developed. The method of calculating the electrical parameters in real time requires the derivation of quadratic equations. Since the circuit has two variants of operation at given parameters, two solutions are obtained, and the correct one must be determined by logical considerations. During simulations, the circuit of resistor elements corresponding to the transmission resistance can be connected, but such a model might be complex with a large number of resistor elements and a longer execution time. It was concluded that the use of a voltage source element that is equivalent to active resistance is the easiest to implement and more rational for simulations of multiple trolleybuses moving along a common overhead catenary stage. Simulation results confirmed the first hypothesis that the increase in drive energy consumption due to the mass of mobile ESS is below 5 % while the substation's total energy consumption might decrease by more than 40 %. As the end of trolleybus acceleration has the highest power consumption and consequently the highest transmission losses, it is recommended that the SC ESS can supply power to the drive until the end of the acceleration mode, thus avoiding the substation power peak. In general, the use of a well-designed mobile SC ESS pays back and the financial return of using ESS is more significant at higher electricity prices than at lower costs of ESS purchase and installation. In some situations, it might be necessary to charge the mobile SC ESS of an electric vehicle from the overhead catenary, for example, by constant current or constant power at the SC input. Detailed calculations by derived expressions based on the RC circuit, which is the most widely used model for real SC replacement, rejected the second hypothesis by finding that charging the SC with constant current at the SC input is more efficient than charging with constant power at the SC input under equal conditions, and the same is true for discharging. Since this difference depends on SC internal resistance and is usually below 1 %, the two methods might be considered almost equivalent, but the finding, which is relevant for SC ESS or RC circuit of any scale, is of fundamental value and also of practical importance since the efficiency of the constant-current method could be more noticeable in the long-term use of SC.

6. REFERENCES

[1] J. J. Mwambeleko, T. Kulworawanichpong, K. A. Greyson, “Tram and trolleybus net traction energy consumption comparison”, 18th International Conference on Electrical Machines and Systems (ICEMS) 2015, Pattaya, Thailand.

[2] L. Hubka, P. Školnik, “Tram Simulation Model for Energy Balance Analyses”, 21st International Conference on Process Control (PC) 2017, Slovakia.

[3] M. Bartlomjczyk, S. Mirchevski, “Reducing of energy consumption in public transport – Results of experimental exploitation of super capacitor energy bank in Gdynia trolleybus system,” 16th International Power Electronics and Motion Control Conference and Exposition (PEMC), 2014.

[4] M. Bartlomiejczyk, “Super capacitor energy bank MEDCOM UCER-01 in Gdynia trolleybus system,” 42nd Annual Conference of the IEEE Industrial Electronics Society, 2016.

[5] M. Bartlomiejczyk, “Modern technologies in energy demand reducing of public transport – practical applications”, 2017.

[6] D. Iannuzzi, P. Pighetti, P. Tricoli, “A study on Stationary Supercapacitor sets for Voltage Droops Compensation of Streetcar Feeder Lines,” Electrical Systems for Aircraft, Railway and Ship Propulsion, 2010.

[7] L. Streit, P. Drabek, “Simulation Model of Tram with Energy Storage System”, 2013.

[8] L. Latkovskis, V. Brazis, “Simulation of the Regenerative Energy Storage with Supercapacitors in Tatra T3A Type Trams”, 2008.

[9] L. Latkovskis, V. Brazis, L. Grigans, “Simulation of On-Board Supercapacitor Energy Storage System for Tatra T3A Type Tramcars”, Modelling Simulation and Optimization. G. Rey, L. Muneta ed. Sciyo: InTech, 2010.

[10] U. Sirmelis, L. Grigans, L. Latkovskis, “An analytic simulation model for a supercapacitor-based energy storage system”, Proceedings of the 14th European Conference on Power Electronics and Applications, 2011, Birmingham, UK.

[11] F. Ciccarelli, A. Del Pizzo, D. Ianuzzi, “Improvement of energy efficiency in light railway vehicles based on power management control of wayside lithium-ion capacitor storage”, IEEE Transactions on Power Electronics, Vol. 29, No. 1, January 2014.

[12] R. Barrero, X. Tackoen, J. Van Mierlo, “Analysis and configuration of supercapacitor-based energy storage system on-board light rail vehicles”, 13th International Power Electronics and Motion Control Conference, 2008, Poznan, Poland.

[13] H. Xia, H. Chen, Z. Yang, F. Lin, B. Wang, “Optimal Energy Management, Location and Size for Stationary Energy Storage System in a Metro Line Based on Genetic Algorithm”, Energies, 2015.

[14] L. Grigāns, “Rekuperētās elektriskās enerģijas izmantošana pilsētas elektrotransportā, pielietojot superkondensatorus”, Summary of the Doctoral Thesis, Riga, 2012.

[15] L. Latkovskis, L. Grigans, “Estimation of the untapped regenerative braking energy in urban electric transportation network”, 13th International Power Electronics and Motion Control Conference, 2008, Poznan, Poland.

[16] L. Grigāns, “Rekuperētās elektriskās enerģijas izmantošana pilsētas elektrotransportā, pielietojot superkondensatorus”, Summary of the Doctoral Thesis, Riga, 2012.
[17] L. Grigans, L. Latkovskis, “Estimation of the power and energy requirements for trackside energy storage systems”, 13th European Conference on Power Electronics and Applications, 2009, Barcelona, Spain.
[18] V. Brazis, G. Zaleskis, L. Latkovskis, L. Grigans, “Traction drive load simulator”, The 52nd Annual International Scientific Conference of Riga Technical University, Riga, Latvia 2011.
[19] P. Drabek, L. Streit, “The energy storage system for public transport vehicles”, 13th European Conference on Power Electronics and Applications, 2009, Barcelona, Spain.
[20] J. F. Pedrayes, M. G. Melero, J. G. Norniella, M. F. Cabanas, G. A. Orcajo, and A. S. González, “Supercapacitors in Constant-Power Applications: Mathematical Analysis for the Calculation of Temperature”, *Appl. Sci.*, vol. 11, no. 21, Art. no. 21, Jan. 2021.
[21] A. Rufer, P. Barrade, “A supercapacitor-Based energy Storage Substation for Voltage Compensation in Weak Transportation Networks”, IEEE Transactions on Power Delivery, 2004.
[22] M. B. Richardson, “Flywheel energy storage system for traction applications,” in Proc. Int. Conf. Power Electron., Mach. Drives, 2002, ISSN 0537-9989, pp. 275–279.
[23] D. R. Kelsall, “Pulsed power provision by high speed composite flywheel,” in *Proc. Pulsed Power Inst. Elect. Eng. Symp.* London, U.K., 0.5 3–4, 2000, INSPEC Acc. No. 6 623 246, pp. 16/1–16/5.
[24] “SITRAS SES, Energy Storage System for 750 V DC Railway,” Siemens Transportation Systems, Public. No. A19100-V300-B276 and B275.
[25] R. Barrero, J. Van Mierlo, X. Tackoen, “Energy Savings in Public Transport: Enhanced Energy Storage Systems for Improved On-Board Light Rail Vehicle Efficiency”, IEEE Vehicular Technology Magazine, 2008.
[26] R. Barrero, X. Tackoen, J. Van Mierlo, “Improving energy efficiency in public transport: stationary supercapacitor-based energy s,torage systems for a metro network”, IEEE Vehicle Power and Propulsion Conference (VPPC), September 3–5, 2008, Harbid, China.
[27] H. Hoimoja, “Energy Efficiency Estimation and Energy Storage Calculation Methods for Urban Electric Transportation”, PhD Thesis, Tallinn University of Technology, Tallin, Estonia, 2009.
[28] U. Sirmelis, “Pilsētas elektrotransporta sistēmu modelēšana optimālu enerģijas uzkrājēju parametru izvēlei”, Summary of the Doctoral Thesis, RTU Press, Riga, 2015.
[29] Y. Wang, Z. Yang, and F. Li, “Optimization of Energy Management Strategy and Sizing in Hybrid Storage System for Tram”, *Energies*, vol. 11, no. 4, Art. no. 4, Apr. 2018.
[30] J. F. Pedrayes *et al.*, “Lambert W function based closed-form expressions of supercapacitor electrical variables in constant power applications”, *Energy*, vol. 218, p. 119364, Mar. 2021.

Ģirts Staņa was born in 1989 in Riga. He received a Bachelor's degree in Electrical Engineering (2013) and a Master's degree in Electrical Engineering (2014) from Riga Technical University. Since 2015, he has worked at the RTU Institute of Industrial Electronics and Engineering (since 1 May 2024 – Institute of Industrial Electronics, Electrical Engineering and Energy) as a research assistant and since 2022 – as a researcher. His research interests include the efficiency of electric transport and energy storage systems.